Influence of cracking and shear connection deformation on the behaviour of steel-concrete composite beams

João Diogo dos Santos Matos Cardoso

Thesis to obtain the Master of Science Degree in

Civil Engineering

Supervisors: Professor Ricardo José de Figueiredo Mendes Vieira

Professor Francisco Baptista Esteves Virtuoso

Examination Committee

Chairperson: Professor José Manuel Matos Noronha da Câmara

Supervisor: Professor Ricardo José de Figueiredo Mendes Vieira

Members of the Committee: Professor Luís Manuel Soares dos Santos Castro

October 2014

Abstract

The effect of the shear connection deformation and of the cracking of the concrete flange on the hogging region are relevant aspects on the global response of steel-concrete composite beams, particularly, in what regards stress redistribution from concrete to steel, longitudinal distribution of shear flow and beam deflection.

An analytical model accounting for the relative displacements at the steel-concrete interface is formulated. The model consists of two Euler-Bernoulli beams coupled by a uniformly distributed spring permitting longitudinal deformation at the interface. The system of differential equations describing the problem of partial interaction is solved and an analytical solution is obtained.

In addition, a model of finite elements for the analysis of composite beams with deformable connection is developed by approaching the displacement fields of the concrete flange and of the steel beam. The results obtained numerically are compared with the corresponding analytical solution so that the validity of the linear numerical model is confirmed.

In order to take into account the influence of the concrete flange's cracking over the hogging regions, a non-linear method of analysis consisting of an incremental and iterative process is adopted. This method permits the implementation of non-linear constitutive laws, namely, those considering the strain-softening behaviour of the concrete under tension or neglecting completely the concrete's tensile strength.

The accuracy of the non-linear model is evaluated by comparing the numerical results with experimental data available in literature.

Keywords:
Steel-concrete composite beams
Deformable connection
Concrete cracking
Finite element method
Non-linear analysis

Resumo

O efeito da deformabilidade da conexão assim como o da fendilhação da peça de betão na zona de momentos negativos são aspectos relevantes na análise do comportamento global de vigas mistas de aço e betão, particularmente no que diz respeito à redistribuição de tensões normais do betão para o aço, à distribuição longitudinal do fluxo de corte na interface aço-betão e aos deslocamentos verticais da viga.

Neste trabalho formula-se um modelo analítico que considera os deslocamentos relativos na interface aço-betão da viga mista. O modelo consiste no acoplamento de duas vigas Euler-Bernoulli através de molas uniformemente distribuídas ao longo da interface aço-betão e considera um comportamento linear para o betão. Apresenta-se a solução analítica de uma viga contínua sujeita a um carregamento uniformemente distribuído para diferentes valores da rigidez de conexão.

Simultaneamente desenvolve-se um modelo de elementos finitos para a análise de vigas mistas com conexão deformável aproximando o campo de deslocamentos no banzo de betão e no perfil metálico. Os resultados obtidos numericamente são comparados com a respectiva solução analítica de modo a que a validade do modelo numérico linear seja confirmada.

De forma a considerar a influência da fendilhação do betão, adopta-se um método de análise não-linear incremental e iterativo que permita a implementação de relações constitutivas não-lineares para o betão, considerando a sua fraca resistência à tracção ou desprezando-a por completo.

A precisão do modelo numérico não-linear é avaliada, comparando os resultados obtidos com resultados experimentais disponíveis na literatura.

Palavras chave:
Vigas mistas aço-betão
Conexão deformável
Fendilhação do betão
Método dos elementos finitos
Análise não linear

Acknowledgements

I would like to express my gratitude to everyone who somehow have contributed to the development of the present work. However, I would also like to address a special thank to:

Professor Ricardo Vieira, my supervisor, for his guidance and scientific contribute. His endeavours were absolutely essential to take this dissertation this far.

Professor Francisco Virtuoso, my co-supervisor, for his advice and foresight, which significantly shaped the final outcome of this thesis.

Professor José Moitinho de Almeida for his helpfulness and aid on the development of the numerical model.

The management and staff of JSJ, for the comprehension and flexibility afforded during the last few weeks.

Rodrigo Borges, for his friendship and also for the linguistic revision.

My close friends, with whom I have shared these last fantastic years, for having been an immeasurable source of motivation and happiness.

Maria, not only for being my dearest person, but also for having inspired me, throughout my whole academic course, to achieve so many things, in particular my position towards life and knowledge.

My parents and sister, who have given me the opportunity to get here and who have always supported me unconditionally.

Contents

List of Figures

Chapter 1

Introduction

Over the last few decades steel-concrete composite structures have been widely applied in building construction, being adopted as floor or wall elements, as well as in bridge construction. The good performance of this structural elements is justified by the ability of employing the best characteristics of each material to the function it is expected to fulfil. Moreover, the composite action is provided by means of locking devices or mechanical connectors which have proven to be reliable and of easy application. Steel and concrete have also a quite similar thermal expansion coefficient which renders their combination even more advantageous.

This work deals specifically with steel-concrete composite beams typically composed by a hot rolled I-beam or a plate girder together with a concrete flange. The two parts are connected to one another through mechanical connectors, being usually adopted headed studs.

The stiffness of a composite beam depends on its degree of interaction. When the shear connection is rigid enough to prevent slip, the interaction between both materials is total, otherwise it is classified as partial interaction. As for resistance, a composite beam is considered to have total connection whenever its ultimate limit state is not determined by the connection capacity. A composite beam is assumed to be in a state of partial connection if its resistance is limited by the shear connectors ultimate strength. Despite being intimately related, the degree of interaction and the degree of connection are quite different concepts dealing with different aspects of the composite beams' behaviour.

The problem of partial interaction and the cracking of the concrete flange on the hogging region of composite beams are the main objectives of this study. In fact, the flexibility of the shear connection plays a crucial role in the overall response of composite beams, particularly in what regards deflection, stress redistribution between the concrete slab and the steel beam and shear flow longitudinal distribution.

A numerical model is developed to evaluate the influence of the partial interaction in composite beams

taking into account the tension stiffening phenomenon. This model is based on the Finite Element Method (FEM), which has presented good qualities in providing reliable results, having been a very useful tool in the study of partial interaction problem [1, 4, 8].

The concrete's non-linear behaviour, particularly under tension, is also taken into account, since it influences significantly the global response of composite beams. In fact, the concrete's cracking over the hogging region leads to a decrease of the composite cross-section stiffness and, hence, to a bending moment redistribution from the inner supports to mid-span.

Time-dependent effects, namely the creep and the shrinkage of the concrete slab, also cause stress redistributions influencing substantially the behaviour of composite beams. Nevertheless, this thesis is only focused on short-term analyses and therefore time-dependent phenomena are considered out of the scope of this work.

The non-linear behaviour in hogging region is both a physical and a geometrical non-linear behaviour. In fact, in addition to concrete's cracking, on hogging regions the steel beam is under compression and therefore buckling phenomena may occur (e.g. local buckling of the web, lateral-torsional buckling due to the compression of the bottom flange).

Since the main aims of this work are to study the influence of the connection's flexibility and evaluate the influence of concrete's cracking on composite beams' behaviour, neither time-dependent effects nor buckling phenomena are accounted for.

Aside from concrete's contitutive law under tension, no other physical non-linearities are considered. Thus, structural steel is assumed to behave in a linear elastic mode. As for the connectors a linear constitutive law based on their secant stiffness corresponding to 50% of their ultimate strength, according to Johnson [9], is also adopted.

In order to fulfil the proposed objectives, a beam finite element is developed to study the influence of the interface connection deformation and the cracking of the concrete slab by a proper constitutive law. The finite element model was implemented under MATLAB environment, having been specifically developed to satisfy this dissertation's aims. Other more sophisticated models (e.g. utilising shell finite elements) and tools (e.g. finite elements commercial programmes) could have been used. However, the good accuracy presented by the adopted model has proven those options to be cumbersome.

The finite element consists of two Euler-Bernoulli beams in planar bending (restraining out-of-plane buckling) coupled by a uniformly distributed spring in order to simulate the mechanical connectors.

A displacement formulation of the FEM is adopted, i.e., the problem is approached by approximating the displacement fields. Therefore, the compatibility is verified at a local level either over the element's domain or at the boundary, whereas the equilibrium is imposed in an average sense over the domain.

The numerical model is validated by comparing the solutions with analytical solutions obtained from the system of differential equations governing the partial interaction problem in composite beams.

The numerical model is adopted to perform a physical non-linear analysis of composite beams. A Newton-Raphson algorithm consisting of an incremental and iterative process in which the structure's response is updated as the load level increases. For each load increment, an iterative procedure is performed globally on the whole structure, until a convergence level, according to an established criterion is achieved.

Once the displacements of the two coupled beams, constituting the composite beam, are determined, the deformation field becomes known. Through the materials' constitutive laws the stresses fields are obtained and by integrating them on the cross section the internal forces, including the shear flow at the steel-concrete interface, are determined. Thus, the composite beam's behaviour is completely defined, and conclusions, about both the influence of the connection's flexibility and the cracking of the concrete flange, can be drawn.

1.1 Brief literature review

A brief literature review is herein presented provided that the problem of composite beams with partial interaction has been approached by a limited number of authors. Yet, since the middle of the last century, analytical and numerical models as well as experimental tests were carried out in order to better evaluate the composite beams behaviour. Some of these works as Newmark's [10], Aribert's [8] or Ansourian's [11] are worth being highlighted.

In 1951, Newmark *et al* [10] formulated the model which has served as basis to almost all the subsequent works dealing with the partial interaction problem. It consist of two Euler-Bernoulli beams coupled by means of a uniformly distributed spring allowing only longitudinal relative displacements. Later on, Adekola [12] proposed a more general model taking into account the vertical relative displacement between the concrete slab and the steel beam, which was observed and measured in experimental tests made by Chapman and Balakrishnan [6] (cited by [1,8]). Adekola has further suggested the model implementation through the finite difference method.

Derived from Newmark's formulation several analytical models, seeking closed-form solutions for the gov-

erning differential equations describing the partial interaction problem, have been proposed to evaluate the influence of the connection deformation in the global response of composite beams within the physical linear range [13–15].

Newmark's hypothesis of assimilating a composite beam to two Euler-Bernoulli beams bonded to one another through longitudinally deformable springs, has also been considered by several authors in order to develop numerical approximate solutions through the FEM theory. Several kinds of one-dimension finite elements were proposed in the last years.

In 1998, Salari *et al* [16] have compared the effectiveness between two different approaches, the approximation of internal forces or the approximation of displacements fields. Both were implemented in a non-linear analysis process, where the forces approximation have exhibited superior ability to perform. However, some difficulties arise in choosing the force interpolation functions. For a statically determinate element, the force interpolation functions resulting from the equilibrium correspond to the exact distribution of internal forces. The existence of a bond force at the interface renders the composite beam in a statically indeterminate element and therefore the choice of those interpolation functions is not trivial. Furthermore, the model approximating the forces field has shown some discontinuities in what regards local compatibility, in much the same way as the displacement based model has shown problems of local equilibrium.

In order to overcome these limitations, in 2000, Ayoub and Filipou [17] developed a two-field mixed element, by approximating independently internal forces and displacement fields, which seems to combine the advantages of both formulations. In this model the two axial forces and the summation of the bending moments on each element were approximated by force interpolation functions whereas the bond force at the interface was described by the displacement field. This new approach was further extended by Dall'Asta and Zona [18], who formulated a three-field mixed finite element based on the approximation of displacements, strains and forces fields.

Regarding long-term analysis, namely the effect of the creep and shrinkage, one of the chief issues of concern in composite beams analysis, numerous works are available in the literature. Dezi and Tarantino [19] (cited by [4, 20]) have developed an analytical model considering the time-dependent behaviour of concrete in the study of composite beams with flexible connection, having proposed its implementation through the finite difference technique. Later on, Amadio [21] as well as Ranzi and Bradford [22] have implemented their numerical model by resorting to finite elements' theory. More recently, Vieira and Virtuoso [23] presented a numerical model of a composite beam with deformable connection, including, not only, the time-dependent effects but also the influence of the concrete cracking. This model was based on a non-conventional finite element formulation, that is, by approximating the internal forces, which has proven to be particularly efficient

for the analysis of the stress redistribution due to concrete cracking over the hogging regions.

Studies on geometrical non-linear effects on composite beams with partial interaction have also been based on the model with two Euler-Bernoulli beams bonded with longitudinal springs proposed by Newmark. Girhammar and Gopu [13] proposed general closed-form solutions of second-order analyses for composite beam-columns subjected to transverse and axial loading. Ranzi *et al* [24] developed a numerical model, within the non-linear finite deformation theory, for composite beams-columns with transverse and longitudinal partial interaction, by approximating the displacement field.

Some modifications to Newmark's kinematical model have been proposed by some authors studying the significance of shear strain, mainly on the steel beam element, in order to evaluate the global response of composite beams with deformable connection. In 2011, Zona and Ranzi [25] tested a new finite element model for physical non-linear analysis of composite beams in combined bending and shear. Firstly, they have assigned a Timoshenko beam only to the steel beam and then to both the concrete slab and the steel part. Through comparison with experimental results this model has proven to be a more suitable tool for short beams with small span-to-depth ratios and with higher levels of shear connection stiffness.

Lately, Nguyen *et al* [15] and Faella *et al* [20] presented a closed-form solution of the governing equations describing the behaviour of a composite beam with deformable shear connection. By so doing, they have formulated an "exact" one-dimension finite element which may be implemented into the usual codes of finite elements analysing composite beams with partial interaction. This new model has exhibited the ability to orientate design in the linear range by utiling only one element per member of a continuous beam.

The model formulated in this work has adopted the Newmark's hypotheses and it was implemented through the finite element method by approximating the displacement field. The model was adopted to study the influence of the structural concrete's cracking and shear connection deformation on the overall response of composite beams. A Serviceability Limit State (SLS) analysis is performed for two different constitutive relations of concrete under tension by considering the strain-softening branch or by neglecting the concrete's resistance.

1.2 Thesis layout

This text is organised in four chapters sorted by the sequence of work adopted, excluding this introductory chapter.

A general analytical model is formulated, in the second chapter. The equilibrium equations, compatibil-

ity conditions and constitutive laws are developed fort a Newmark type of model. This general model encompasses the shear deformation of both elements, steel and concrete, and allows transverse relative displacements between them. A simplification of Newmark's model is formulated, by restraining the uplift and neglecting the shear deformation, since one of the main objectives of this work is to evaluate the effect of the interface connection deformation on the axial stress redistribution between the concrete slab and the steel beam.

So far all materials are considered to behave linear elastically so that the system of differential equations governing the problem of partial interaction is analytically solvable and the numerical results provided by finite elements can be compared with an analytical solution.

Thereafter, in chapter three, a finite element is formulated, by approximating the displacements field. Some practical examples, e.g. simply supported and two-span continuous beams, are performed in order to validate numerical results with analytical solutions. Hence, some conclusions regarding the performance of the adopted finite element can be drawn. On the other hand, the influence of the interface connection stiffness can also be evaluated.

In the fourth chapter, the concrete's non-linear constitutive law is briefly described and the incremental and iterative procedure underlying its implementation is explained. In order to validate the non-linear analysis model presented in this chapter, experimental results for simply supported beams published by [6] in 60's and for continuous beams presented by Ansourian [11] in early 80's are used as benchmark.

Furthermore, the response of an arbitrary composite beam evaluated according to EN 1994 is compared with the corresponding results obtained by the proposed numerical model considering either the descending branch representing the strain-softening behaviour or neglecting the concrete under tension at all.

Finally, in the fifth chapter, the most relevant conclusions are presented and some ideas, which have appeared to be pertinent in the course of this work, are proposed for future developments.

Chapter 2

Linear analysis of composite beams with longitudinal partial interaction

2.1 Introduction

A formulation for the structural analysis of steel-concrete composite beams with deformable shear connection is presented in this section.

A general analytical model is derived from the formulation of the compatibility, the equilibrium and the constitutive laws, describing the behaviour of an infinitesimal interval of a composite beam. This model consists of two Euler-Bernoulli beam elements coupled at the interface connection modelled by means of a uniformly distributed spring which deforms longitudinally along the beam length, transversely to the connection interface, and rotationally, turning about the beam bending axis. The longitudinal and transverse deformations at the connection interface are, respectively, referred to as *slip* and *uplift*. This terms have been widely spread out in the literature dealing with composite beams, and are adopted in this work.

Since the influence of the partial interaction is the main objective of this chapter the non-linear physical behaviour is not considered, being all the intervenient materials assumed to behave in a linear elastic manner.

A more simplified kinematical model, known as Newmark's model [10] (cited by [1, 26, 27]), which neglects the shear deformation of both elements and takes solely into account the longitudinal deformation of the interface connection, is adopted.

An analytical solution deriving from the developed model is presented and an illustrative example of a continuous composite beam subjected to a uniformly distributed load is solved for different practical values

of a connection stiffness parameter.

2.2 General analytical model

2.2.1 Basic assumptions

A steel-concrete composite beam is represented in figure 2.1, being adopted as reference an orthonormal system $\{O;\ X,\ Y,\ Z\}$. The beam is composed by two elements and occupies the spatial region $V = A \times L$, in which A represents its cross section and L the beam length. The composite cross section is formed by two parts with areas A_1 and A_2, corresponding to the concrete slab and to the steel girder, which for ease of notation are referred to as elements 1 and 2, respectively. The cross section is orthogonal to the X axis and symmetric about the bending plane XZ. z_c is the z coordinate of the interface between the two elements and $z_1,\ z_2$ are the respective z coordinates of the centroids of elements 1 and 2. The unit vectors corresponding to the axis $X,\ Y,\ Z$ are represented by **i, j, k**, respectively.

In spite of being obtained by a set of connectors with a discrete distribution, the connection between the two elements is assumed to be continuously distributed over the steel-concrete interface, without any loss of validity [16, 28](cited by [4]). This connection provides the composite behaviour, though it permits relative displacements in both longitudinal and transverse directions, which are known, respectively, as longitudinal slip and vertical uplift.

The Bernoulli's hypothesis is assumed to be valid for each element of the composite beam, that is, plane sections remain plane except for a relative displacement at the two elements interface. No torsional or out-of-plane flexural effects are taken into account.

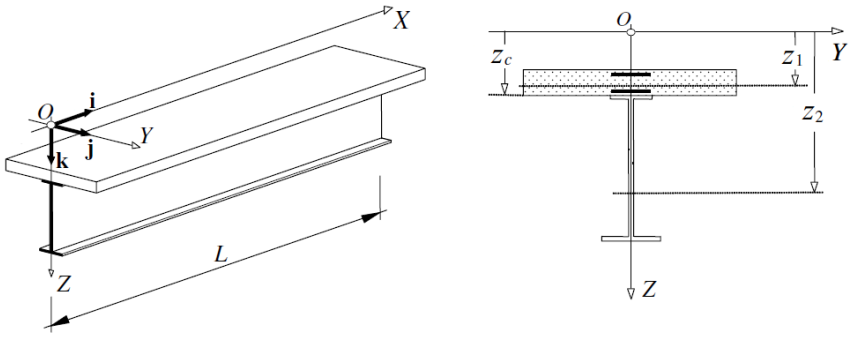

Figure 2.1: Composite beam and cross section (adapted from [1]).

2.2.2 Compatibility conditions

Based on Newmark's derived model, the kinematical model adopted to describe the behaviour of the composite beam considers plane sections to remain plane except for a relative displacement at the connection interface. Hence, in order to represent the behaviour of the beam, one must know all the variables of the corresponding displacement field, which is represented by the vector $\mathbf{d}$ as follows.

$$\mathbf{d}^T = \begin{bmatrix} u_1(x) & w_1(x) & \theta_1(x) & u_2(x) & w_2(x) & \theta_2(x) \end{bmatrix}$$

where $u_1(x),\ w_1(x),\ \theta_1(x),\ u_2(x),\ w_2(x)$ and $\theta_2(x)$ represent the axial displacement, the vertical displacements and the rotations at the centroid of elements 1 and 2, respectively. For ease of notation the displacements will be referred to as $u_1,\ w_1,\ \theta_1,\ u_2,\ w_2$ and θ_2. The displacement of an arbitrary point of the element α (with $\alpha = 1,\ 2$) can then be defined by the following vectors:

$$\mathbf{u}_\alpha(x,z) = w_\alpha \mathbf{k} + [u_\alpha + (z - z_\alpha)\theta_\alpha]\mathbf{i} \quad \text{on } A_\alpha, \forall x \in [0, L] \tag{2.2.1}$$

Since the small displacements hypothesis is considered to be valid, the non-null strain components are given by:

$$\boldsymbol{\varepsilon}_\alpha(x,z) = \frac{\partial \mathbf{u}_\alpha(x,z)}{\partial x} \cdot \mathbf{i} = \frac{du_\alpha}{dx} + (z - z_\alpha)\frac{d\theta_\alpha}{dx} \quad \text{on } A_\alpha, \forall x \in [0, L] \tag{2.2.2}$$

$$\boldsymbol{\gamma}_\alpha(x) = \frac{\partial \mathbf{u}_\alpha(x,z)}{\partial z} \cdot \mathbf{i} + \frac{\partial \mathbf{u}_\alpha(x,z)}{\partial x} \cdot \mathbf{k} = \theta_\alpha + \frac{dw_\alpha}{dx} \quad \text{on } A_\alpha, \forall x \in [0, L] \tag{2.2.3}$$

$$\chi_\alpha(x) = \frac{d\theta_\alpha}{dx} \quad \forall x \in [0, L] \tag{2.2.4}$$

where $\boldsymbol{\varepsilon}_\alpha(x,z),\ \boldsymbol{\gamma}_\alpha(x)$ and $\chi_\alpha(x)$ are, respectively, the axial strain, the shear strain on the plane XZ and the curvature of the element α.

For the complete kinematical description of the composite beam, relative displacements at the steel-concrete interface have also to be accounted for in the strain field. The adopted kinematical model is presented in figure 2.2.

The relative displacements at the connection interface are expressed by the $\boldsymbol{\delta}$ vector.

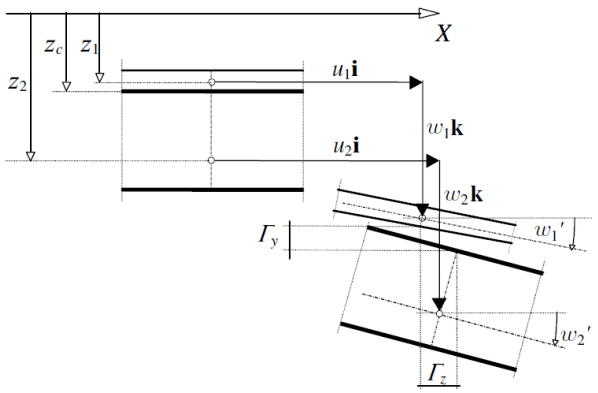

Figure 2.2: Kinematical model (adapted from)

$$\boldsymbol{\delta}(x) = \delta_x(x)\mathbf{i} + \delta_\theta(x)\mathbf{j} + \delta_z(x)\mathbf{k} = (u_2 + z_{c2}\theta_2 - u_1 - z_{c1}\theta_1)\mathbf{i} + (\theta_2 - \theta_1)\mathbf{j} + (w_2 - w_1)\mathbf{k} \quad \forall x \in [0, L] \quad (2.2.5)$$

where δ_x, δ_z and δ_θ represent, respectively, the longitudinal slip, the transverse uplift and the relative rotation between the two elements; $z_{c1} = z_c - z_1$ and $z_{c2} = z_c - z_2$, and z_{c1} and z_{c2} can be positive or negative depending on the adopted reference system as shown in figure 2.1.

The strain field can be defined as a function of a deformation parameters vector whose components depend solely on the x coordinate of the section. These deformation parameters correspond to the axial strain at the fibres located at z_α, shear strain, curvature and to the relative displacements at the connection interface.

$$\varepsilon_\alpha \equiv \varepsilon_\alpha(x, z_\alpha) = \frac{du_\alpha}{dx} \quad (2.2.6)$$

$$\gamma_\alpha \equiv \boldsymbol{\gamma}_\alpha(x) \quad (2.2.7)$$

$$\chi_\alpha \equiv \chi_\alpha(x) \quad (2.2.8)$$

$$\delta_x \equiv \delta_x(x) \quad (2.2.9)$$

$$\delta_z \equiv \delta_z(x) \quad (2.2.10)$$

$$\delta_\theta \equiv \delta_\theta(x) \quad (2.2.11)$$

Thus, the strain field can be expressed by:

$$\boldsymbol{\varepsilon} = \mathbf{E}\ \mathbf{e} \quad (2.2.12)$$

in which $\boldsymbol{\varepsilon}$ is the strain field, $\mathbf{e}$ is the vector of the deformation parameters and $\mathbf{E}$ represents the deformation

modes matrix.

$$\boldsymbol{\varepsilon}^T = \begin{bmatrix} \boldsymbol{\varepsilon}_1(x,z) & \boldsymbol{\gamma}_1(x) & \boldsymbol{\varepsilon}_2(x,z) & \boldsymbol{\gamma}_2(x) & \delta_x & \delta_z & \delta_\theta \end{bmatrix}$$

$$\mathbf{e}^T = \begin{bmatrix} \varepsilon_1 & \gamma_1 & \chi_1 & \varepsilon_2 & \gamma_2 & \chi_2 & \delta_x & \delta_z & \delta_\theta \end{bmatrix}$$

$$\mathbf{E} = \begin{bmatrix} 1 & \cdot & z-z_1 & \cdot & \cdot & \cdot & \cdot & \cdot & \cdot \\ \cdot & 1 & \cdot & \cdot & \cdot & \cdot & \cdot & \cdot & \cdot \\ \cdot & \cdot & \cdot & 1 & \cdot & z-z_2 & \cdot & \cdot & \cdot \\ \cdot & \cdot & \cdot & \cdot & 1 & \cdot & \cdot & \cdot & \cdot \\ \cdot & \cdot & \cdot & \cdot & \cdot & \cdot & 1 & \cdot & \cdot \\ \cdot & \cdot & \cdot & \cdot & \cdot & \cdot & \cdot & 1 & \cdot \\ \cdot & \cdot & \cdot & \cdot & \cdot & \cdot & \cdot & \cdot & 1 \end{bmatrix}$$

The compatibility equations that define each generalised strain can be rewritten in a matrix form as:

$$\mathbf{e} = \mathscr{D}\mathbf{d} \tag{2.2.13}$$

where $\mathbf{d}$ represents the displacement field, previously defined, and $\mathscr{D}$ is a compatibility differential operator defined as follows.

$$\mathscr{D} = \begin{bmatrix} \frac{d}{dx} & \cdot & \cdot & \cdot & \cdot & \cdot \\ \cdot & \frac{d}{dx} & 1 & \cdot & \cdot & \cdot \\ \cdot & \cdot & \frac{d}{dx} & \cdot & \cdot & \cdot \\ \cdot & \cdot & \cdot & \frac{d}{dx} & \cdot & \cdot \\ \cdot & \cdot & \cdot & \cdot & \frac{d}{dx} & 1 \\ \cdot & \cdot & \cdot & \cdot & \cdot & \frac{d}{dx} \\ -1 & \cdot & -z_{c1} & 1 & \cdot & z_{c2} \\ \cdot & -1 & \cdot & \cdot & 1 & \cdot \\ \cdot & \cdot & -1 & \cdot & \cdot & 1 \end{bmatrix}$$

2.2.3 Equilibrium equations

A composite beam is assumed to be subjected to arbitrary axial and transverse uniformly distributed forces ($p_{x1},\ p_{x2},\ p_{z1},\ p_{z2}$) and moments ($m_1,\ m_2$) as represented in figure 2.3. The respective connection forces ($f_x,\ f_z,\ f_\theta$) are developed along the interface between the two elements.

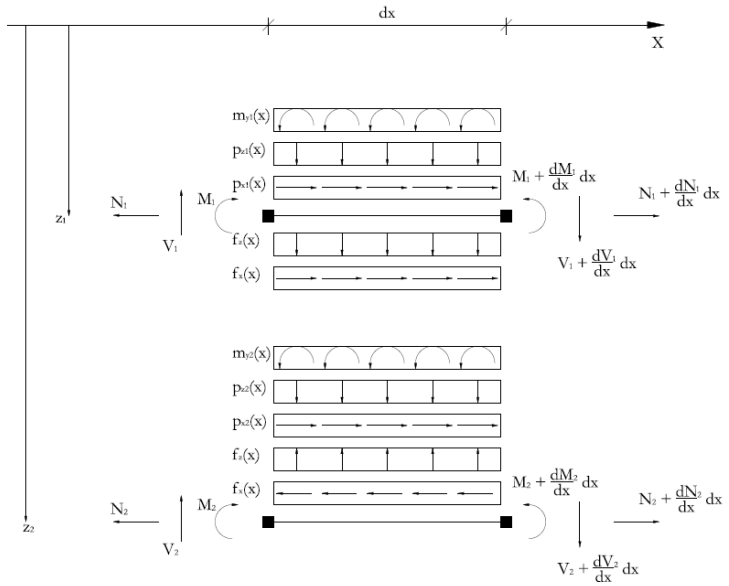

Figure 2.3: Free-body diagram of an infinitesimal segment of a composite beam.

Equilibrium differential equations can be established for both elements, according to the free-body diagram presented in Figure 2.3.

$$\frac{dN_1}{dx} + p_{x1} + f_x = 0 \tag{2.2.14}$$

$$\frac{dV_1}{dx} + p_{z1} + f_z = 0 \tag{2.2.15}$$

$$\frac{dM_1}{dx} - V_1 + m_1 + z_{c1} f_x + f_\theta = 0 \tag{2.2.16}$$

$$\frac{dN_2}{dx} + p_{x2} - f_x = 0 \tag{2.2.17}$$

$$\frac{dV_2}{dx} + p_{z2} - f_z = 0 \tag{2.2.18}$$

$$\frac{dM_2}{dx} - V_2 + m_2 - z_{c2} f_x - f_\theta = 0 \tag{2.2.19}$$

where N_1, V_1, M_1, N_2, V_2 and M_2 represent the internal axial forces, shear forces and bending moments acting on the concrete and steel components, respectively. Rewriting equations 2.2.14 to 2.2.19 in their matrix form, the following equation is obtained:

$$\mathscr{D}^* \mathbf{s} + \mathbf{p} = \mathbf{0} \tag{2.2.20}$$

where $\mathbf{s}$ represents the internal forces vector and $\mathbf{p}$ the span loads vector given by:

$$\mathbf{s}^T = \begin{bmatrix} N_1 & V_1 & M_1 & N_2 & V_2 & M_2 & f_x & f_z & f_\theta \end{bmatrix}$$

$$\mathbf{p}^T = \begin{bmatrix} p_{x1} & p_{z1} & m_1 & p_{x2} & p_{z2} & m_2 \end{bmatrix}$$

The equilibrium differential operator being self-adjoint[1] of $\mathscr{D}$ is defined as:

$$\mathscr{D}^* = \begin{bmatrix} \frac{d}{dx} & \cdot & \cdot & \cdot & \cdot & \cdot & 1 & \cdot & \cdot \\ \cdot & \frac{d}{dx} & \cdot & \cdot & \cdot & \cdot & \cdot & 1 & \cdot \\ \cdot & -1 & \frac{d}{dx} & \cdot & \cdot & \cdot & z_{c1} & \cdot & 1 \\ \cdot & \cdot & \cdot & \frac{d}{dx} & \cdot & \cdot & -1 & \cdot & \cdot \\ \cdot & \cdot & \cdot & \cdot & \frac{d}{dx} & \cdot & \cdot & -1 & \cdot \\ \cdot & \cdot & \cdot & \cdot & -1 & \frac{d}{dx} & \cdot & -z_{c2} & -1 \end{bmatrix}$$

2.2.4 Constitutive law

The constitutive laws, which describe the relation between stresses and strains for the materials and the connection forces with the amplitude of the deformation along the interface, are considered to be linear elastic.

[1] $d_{ij} = (-1)^{k+1} d^*_{ji}$

The constitutive laws for both materials can be compactly written by the following equation:

$$\boldsymbol{\sigma} = \mathbf{C}\boldsymbol{\varepsilon} \tag{2.2.21}$$

where $\boldsymbol{\sigma}$ represents the stress field in the concrete slab and steel girder, corresponding to elements 1 and 2, respectively, and $\boldsymbol{\varepsilon}_m$ represents the strain field for both elements.

$$\boldsymbol{\sigma}^T = \begin{bmatrix} \sigma^1_{xx}(x,z) & \sigma^1_{xz}(x,z) & \sigma^2_{xx}(x,z) & \sigma^2_{xz}(x,z) \end{bmatrix}$$

$$\boldsymbol{\varepsilon}^T = \begin{bmatrix} \boldsymbol{\varepsilon}_1(x,z) & \boldsymbol{\gamma}_1(x) & \boldsymbol{\varepsilon}_2(x,z) & \boldsymbol{\gamma}_2(x) \end{bmatrix}$$

The matrix $\mathbf{C}$, which relates the stress and strain fields, stores the Young's and shear moduli associated with each element of the composite cross section.

$$\mathbf{C} = \begin{bmatrix} E_1 & \cdot & \cdot & \cdot \\ \cdot & \eta_1 G_1 & \cdot & \cdot \\ \cdot & \cdot & E_2 & \cdot \\ \cdot & \cdot & \cdot & \eta_2 G_2 \end{bmatrix} \quad with \quad \eta_\alpha = \frac{A'_\alpha}{A_\alpha}$$

Where η_α constitutes the coefficient relating the shear area A' with the effective area A of the component α of the composite beam.

The Hooke's law, given by equation 2.2.21, establishes a relation between continuous variables, namely the stress field and the strain field. However, a similar relation between the internal forces and the corresponding deformations located at an arbitrary section of the beam is also required.

From the linear theory of elasticity one knows that the elastic potential energy produced by the internal forces associated with a particular strain field must be equivalent to the potential energy produced by the corresponding stress field. This equivalence is stated in the following form:

$$\mathbf{s}^T\mathbf{e} = \int_A \boldsymbol{\sigma}^T\boldsymbol{\varepsilon}\ dA = \int_A \boldsymbol{\varepsilon}^T\mathbf{C}\boldsymbol{\varepsilon}\ dA = \int_A \mathbf{e}^T\mathbf{E}^T\mathbf{C}\mathbf{E}\ \mathbf{e}\ dA \tag{2.2.22}$$

$$\Leftrightarrow \mathbf{s} = \int_A \mathbf{E}^T\mathbf{C}\mathbf{E}\ dA\ \mathbf{e} = \mathbf{K}\mathbf{e} \tag{2.2.23}$$

being $\mathbf{s}$ the vector of the internal forces, $\mathbf{e}$ the vector of the deformations parameters and $\mathbf{E}$ the deformation modes matrix, accounting for the steel and concrete parts and excluding the connection interface.

$$\mathbf{s}^T = \begin{bmatrix} N_1 & V_1 & M_1 & N_2 & V_2 & M_2 \end{bmatrix}$$

$$\mathbf{e}^T = \begin{bmatrix} \varepsilon_1 & \gamma_1 & \chi_1 & \varepsilon_2 & \gamma_2 & \chi_2 \end{bmatrix}$$

$$\mathbf{E} = \begin{bmatrix} 1 & \cdot & z-z_1 & \cdot & \cdot & \cdot \\ \cdot & 1 & \cdot & \cdot & \cdot & \cdot \\ \cdot & \cdot & \cdot & 1 & \cdot & z-z_2 \\ \cdot & \cdot & \cdot & \cdot & 1 & \cdot \end{bmatrix}$$

The cross-sectional stiffness matrix of the two layers follows from equation 2.2.23:

$$\mathbf{K} = \int_A \mathbf{E}^T\mathbf{C}\mathbf{E}\ dA = \begin{bmatrix} E_1A_1 & \cdot & E_1S_1 & \cdot & \cdot & \cdot \\ \cdot & G_1A_1' & \cdot & \cdot & \cdot & \cdot \\ E_1S_1 & \cdot & E_1I_1 & \cdot & \cdot & \cdot \\ \cdot & \cdot & \cdot & E_2A_2 & \cdot & E_2S_2 \\ \cdot & \cdot & \cdot & \cdot & G_2A_2' & \cdot \\ \cdot & \cdot & \cdot & E_2S_2 & \cdot & E_2I_2 \end{bmatrix} \tag{2.2.24}$$

where $A_\alpha,\ S_\alpha,\ I_\alpha$ are, respectively, the cross-sectional area, first and second moments of area.

$$A_\alpha = \int_{A_\alpha} dA_\alpha, \qquad S_\alpha = \int_{A_\alpha} (z-z_\alpha)dA_\alpha, \qquad I_\alpha = \int_{A_\alpha} (z-z_\alpha)^2 dA_\alpha$$

The constitutive laws for the interface connection in each direction are defined by the following equation:

$$\mathbf{f} = \mathbf{k}_c \boldsymbol{\delta} \tag{2.2.25}$$

where $\mathbf{f}$ represents the interface connection forces,

$$\mathbf{f}^T = \begin{bmatrix} f_x & f_z & f_\theta \end{bmatrix}$$

$\boldsymbol{\delta}$ is the vector of the relative displacements at the steel-concrete interface defined in equation 2.2.5 and $\mathbf{k}_c$ stores the connection stiffness.

$$\mathbf{k}_c = \begin{bmatrix} \rho_x & \cdot & \cdot \\ \cdot & \rho_z & \cdot \\ \cdot & \cdot & \rho_\theta \end{bmatrix}$$

The constitutive laws for the whole composite cross section can be written from the equations 2.2.23 and 2.2.25 as follows.

$$\mathbf{s} = \mathbf{K}\mathbf{e} \tag{2.2.26}$$

where $\mathbf{K}$ is the stiffness matrix which includes all the elastic cross-sectional properties.

$$\mathbf{K} = \begin{bmatrix} E_1A_1 & \cdot & E_1S_1 & \cdot & \cdot & \cdot & \cdot & \cdot & \cdot \\ \cdot & G_1A_1' & \cdot & \cdot & \cdot & \cdot & \cdot & \cdot & \cdot \\ E_1S_1 & \cdot & E_1I_1 & \cdot & \cdot & \cdot & \cdot & \cdot & \cdot \\ \cdot & \cdot & \cdot & E_2A_2 & \cdot & E_2S_2 & \cdot & \cdot & \cdot \\ \cdot & \cdot & \cdot & \cdot & G_2A_2' & \cdot & \cdot & \cdot & \cdot \\ \cdot & \cdot & \cdot & E_2S_2 & \cdot & E_2I_2 & \cdot & \cdot & \cdot \\ \cdot & \cdot & \cdot & \cdot & \cdot & \cdot & \rho_x & \cdot & \cdot \\ \cdot & \cdot & \cdot & \cdot & \cdot & \cdot & \cdot & \rho_z & \cdot \\ \cdot & \cdot & \cdot & \cdot & \cdot & \cdot & \cdot & \cdot & \rho_\theta \end{bmatrix}$$

2.3 Simplified analytical model

For the sake of simplicity, the proposed analytical model does not consider the shear deformation of the composite cross section. Furthermore, the vertical and rotational connection forces along the beam length, considered on the equilibrium equations, are both neglected due to the high complexity of their quantification. Thus, the focus of this chapter is on the longitudinal slip and on the resulting stress distributions.

The assumption of the Bernoulli hypothesis for the two parts of the composite beam has been widely accepted by most authors. Indeed, for the usual dimensions adopted in composite beams' design, with slenderness values (defined as the ratio between the beam longitudinal length and its cross section depth) higher than 10, the shear deformation is not significant, [4, 16, 26, 28].

Some studies available in the literature [8, 29] have proven through numerical and experimental tests that the uplift between the concrete slab and the steel beam has a negligible effect in what regards the slip distribution along the connection interface as well as its load capacity. Since the uplift is restrained, the vertical displacement of both elements must be equal and therefore, by compatibility, their rotations must also be the same.

The equation of shear strain, which becomes null, originates the following relation:

$$\gamma_\alpha = \theta_\alpha + \frac{dw_\alpha}{dx} = 0 \Leftrightarrow \theta_\alpha = -\frac{dw_\alpha}{dx} \tag{2.3.1}$$

Moreover, from now on, since the shear deformation is neglected, one can assume plane sections to remain plane and orthogonal to the beams axis, in the domain of each element, as illustrated in figure 2.4.

According to the compatibility condition which gives the expression for the curvature, it follows that:

$$\chi_\alpha = \frac{d\theta_\alpha}{dx} = -\frac{d^2 w_\alpha}{dx^2} \tag{2.3.2}$$

As the vertical uplift and the relative rotation between both elements are assumed to be null:

$$w_1 = w_2 = w \tag{2.3.3}$$

$$\theta_1 = \theta_2 = \theta \tag{2.3.4}$$

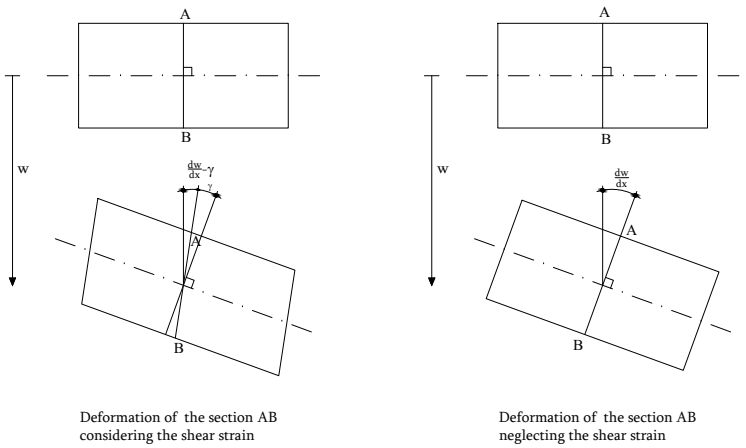

Figure 2.4: Deformation of the section AB.

Thus, equations 2.2.5 and 2.3.2 can be rewritten as follows.

$$\boldsymbol{\delta}(x) = \delta_x \equiv \delta = u_2 - u_1 + h\frac{dw}{dx} \tag{2.3.5}$$

$$\chi_1 = \chi_2 = \chi = \frac{d^2w}{dx^2} \tag{2.3.6}$$

where $h = z_2 - z_1$.

Similarly to equation 2.2.13, the simplified compatibility conditions are written on its matrix form as:

$$\mathbf{e}_s = \mathscr{D}_s \mathbf{d}_s \tag{2.3.7}$$

in which $\mathbf{e}_s$ and $\mathbf{d}_s$ are reduced to:

$$\mathbf{e}_s^T = \begin{bmatrix} \varepsilon_1 & \varepsilon_2 & \chi & \delta \end{bmatrix}$$

$$\mathbf{d}_s^T = \begin{bmatrix} u_1 & u_2 & w \end{bmatrix}$$

and $\mathscr{D}_s$ becomes:

$$\mathscr{D}_s = \begin{bmatrix} \frac{d}{dx} & . & . \\ . & \frac{d}{dx} & . \\ . & . & -\frac{d^2}{dx^2} \\ -1 & 1 & h\frac{d}{dx} \end{bmatrix}$$

As the shear deformation is neglected the shear force does not need to be explicitly considered in the equilibrium equations. By differentiating the sum of equations 2.2.16 and 2.2.19 and substituting equations 2.2.15 and 2.2.18 into the latter ones, it follows that:

$$\frac{d^2M}{dx^2} + p_z + \frac{dm}{dx} + h\frac{df_x}{dx} = 0 \tag{2.3.8}$$

where $M = M_1 + M_2$; $p_z = p_{z1} + p_{z2}$ and $m = m_1 + m_2$.

The three equilibrium equations can be written in a compact form as follows.

$$\mathscr{D}_s^* \mathbf{s}_s - \mathscr{H}^* \mathbf{p}_s = \mathbf{0} \tag{2.3.9}$$

in which $\mathbf{s}_s$ and $\mathbf{p}_s$ become:

$$\mathbf{s}_s^T = \begin{bmatrix} N_1 & N_2 & M & f_x \end{bmatrix}$$

$$\mathbf{p}_s^T = \begin{bmatrix} p_{x1} & p_{x2} & p_z & m \end{bmatrix}$$

$\mathscr{D}_s^*$, being self-adjointed to the compatibility differential operator takes the form:

$$\mathscr{D}_s^* = \begin{bmatrix} \frac{d}{dx} & \cdot & \cdot & 1 \\ \cdot & \frac{d}{dx} & \cdot & -1 \\ \cdot & \cdot & \frac{d^2}{dx^2} & h\frac{d}{dx} \end{bmatrix}$$

$\mathscr{H}^*$ is self-adjointed to a differential operator $\mathscr{H}$ which is defined as:

$$\mathscr{H} = \begin{bmatrix} 1 & \cdot & \cdot \\ \cdot & 1 & \cdot \\ \cdot & \cdot & 1 \\ \cdot & \cdot & -\frac{d}{dx} \end{bmatrix}$$

For the sake of the complete description of the problem eight boundary conditions must be specified.

$$u_\alpha(x) - \bar{u}_\alpha = 0 \quad on \quad \Gamma_u \tag{2.3.10a}$$

$$\frac{dw(x)}{dx} + \bar{\theta} = 0 \quad on \quad \Gamma_\theta \tag{2.3.10b}$$

$$w(x) - \bar{w} = 0 \quad on \quad \Gamma_w \tag{2.3.10c}$$

$$N_\alpha(x) - \bar{N}_\alpha = 0 \quad on \quad \Gamma_N \tag{2.3.10d}$$

$$M(x) - \bar{M} = 0 \quad on \quad \Gamma_M \tag{2.3.10e}$$

$$\frac{dM(x)}{dx} + m + hf_x(x) - \bar{V} = 0 \quad on \quad \Gamma_V \tag{2.3.10f}$$

where Γ and the respective subscript denote the different kind of physical end conditions; $\bar{N}_\alpha$ is the concen-

trated horizontal load applied to the element α, and $\bar{V}$, $\bar{M}$ are the concentrated vertical load and bending moment applied to the composite beam. Either the load or the displacement can be prescribed at a boundary point, but not both. Equations 2.3.10 express the kinematical (essential) boundary condition when the displacements are prescribed or their dual static (natural) boundary conditions when the load is prescribed. As for the constitutive laws, they can be obtained as previously, but now disregarding the shear deformation of each element and either the vertical and rotational connection stiffness. Thus, the generalised constitutive law takes the form:

$$\mathbf{s}_s = \mathbf{K}_s \mathbf{e}_s \tag{2.3.11}$$

where the stiffness matrix of the composite cross section, $\mathbf{K}_s$, is given by:

$$\mathbf{K}_s = \begin{bmatrix} \mathbf{K}_{sm} & \cdot \\ \cdot & \rho_x \end{bmatrix} \tag{2.3.12}$$

being $\mathbf{K}_{sm}$ the stiffness matrix associated with both materials,

$$\mathbf{K}_{sm} = \int_A \mathbf{E}_s^T \mathbf{C}_s \mathbf{E}_s \, dA = \begin{bmatrix} E_1 A_1 & \cdot & \cdot \\ \cdot & E_2 A_2 & \cdot \\ \cdot & \cdot & EI_0 \end{bmatrix} \tag{2.3.13}$$

with $EI_0 = E_1 I_1 + E_2 I_2$. $\mathbf{C}_s$ stores the Young's moduli and $\mathbf{E}_s$ is the respective matrix of the deformation modes.

$$\mathbf{C}_s = \begin{bmatrix} E_1 & \cdot \\ \cdot & E_2 \end{bmatrix}$$

$$\mathbf{E}_s = \begin{bmatrix} 1 & \cdot & z - z_1 \\ \cdot & 1 & z - z_2 \end{bmatrix}$$

2.4 Analytical solution

Equations 2.2.14 to 2.2.19 were formerly written in terms of internal forces. Assuming the physical linearity hypothesis, the same equations can be rewritten as functions of the displacements.

Thus, substituting the compatibility conditions 2.3.7 and the constitutive laws 2.3.11 into the equilibrium equation 2.3.9 the latter takes the form:

$$\mathscr{D}_s^* \mathbf{K}_s \mathscr{D}_s \mathbf{d}_s - \mathscr{H}^* \mathbf{p}_s = \mathbf{0} \tag{2.4.1}$$

The development of the equation 2.4.1 yields the following equilibrium differential equations:

$$E_1 A_1 \frac{d^2 u_1}{dx^2} + \rho_x \left(u_2 - u_1 + h \frac{dw}{dx} \right) = -p_{x1} \tag{2.4.2a}$$

$$E_2 A_2 \frac{d^2 u_2}{dx^2} - \rho_x \left(u_2 - u_1 + h \frac{dw}{dx} \right) = -p_{x2} \tag{2.4.2b}$$

$$-EI_0 \frac{d^4 w}{dx^4} + h\rho_x \left(\frac{du_2}{dx} - \frac{du_1}{dx} + h \frac{d^2 w}{dx^2} \right) = -p_z - \frac{dm}{dx} \tag{2.4.2c}$$

Taking into account only the homogenised form of equations 2.4.2, they can be solved in order to come to their general solution.

$$u_1^{\mathrm{v}} - \alpha^2 u_1''' = 0 \tag{2.4.3a}$$

$$w''' = \frac{\lambda}{h} u_1'' - \frac{\zeta}{h} u_1^{\mathrm{iv}} \tag{2.4.3b}$$

$$u_2 = u_1 - \zeta u_1'' - h w' \tag{2.4.3c}$$

in which the primes and Roman numerals denote the derivative order with respect to the x coordinate and the constants α, λ and ζ are functions of the mechanical and geometrical cross-sectional properties, being defined as:

$$\alpha^2 = \rho_x \left(\frac{EA_0}{E_1 A_1 E_2 A_2} + \frac{h^2}{EI_0} \right); \quad \lambda = \frac{EA_0}{E_2 A_2}; \quad \zeta = \frac{E_1 A_1}{\rho_x}$$

with $EA_0 = E_1 A_1 + E_2 A_2$.

It is worthy of note that H/λ corresponds to the distance of the centroid of the transformed cross-sectional area of the fully composite section, i.e. assuming the connection stiffness to be infinite, from the centroid of the top element.

The governing equations 2.4.3 are established so that they can be solved by direct substitution, that is, the solution of equation 2.4.3b depends solely upon the solution of equation 2.4.3a, and by its turn, the solution of equation 2.4.3c depends on the solutions of equations 2.4.3a and 2.4.3b.

The general solution of the governing equations 2.4.3 takes the following form.

$$u_1(x) = C_1 + C_2 x + C_3 x^2 + C_4 e^{-\alpha x} + C_5 e^{\alpha x} \tag{2.4.4a}$$

$$w(x) = (C_4 e^{-\alpha x} - C_5 e^{\alpha x}) \left(\frac{\zeta \alpha^2 - \lambda}{h\alpha} \right) + \frac{1}{3} \frac{\lambda C_3 x^3}{h} + \frac{1}{2} \frac{\lambda C_2 x^2}{h} + \left(\frac{\lambda C_1 - 2\zeta C_3}{h} \right) x + \frac{1}{2} C_6 x^2 + C_7 x + C_8 \tag{2.4.4b}$$

$$u_2(x) = (1 - \lambda)(C_1 + C_2 x + C_3 x^2 + C_4 e^{-\alpha x} + C_5 e^{\alpha x}) - h(C_6 x + C_7) \tag{2.4.4c}$$

Girhammar [13] and Vieira [4] have presented similar solutions to 2.4.4, depending on the eight constants, C_1 to C_8, which can be determined prescribing the boundary conditions.

An illustrative example of a composite continuous beam with two equal spans and subjected to a unitary

distributed load is shown in 2.5. The composite beam is 24 m long and its cross section is formed by a rectangular concrete slab of class C30/37 and dimension 1500 mm x 150 mm, and a hot rolled steel beam IPE500 of grade S275. A symmetry simplification is adopted.

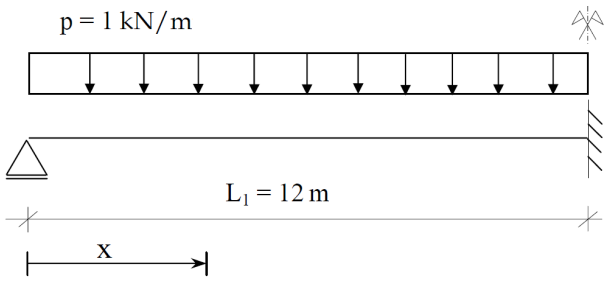

Figure 2.5: Two-span continuous beam (model with symmetry simplification) subjected to a unitary distributed load.

Once the beam is loaded, one must replace the equation 2.4.3a by the following one.

$$u_1^{\mathrm{v}} - \alpha^2 u''' = -\beta p \tag{2.4.5}$$

where

$$\beta = \frac{\rho_x h}{E_1 A_1 E I_0}$$

The solution of 2.4.5 results from the sum of the general solution 2.4.4 with the particular solution taken by:

$$u_{1_p}(x) = \frac{1}{6}\frac{\beta p x^3}{\alpha^2} \tag{2.4.6}$$

The kinematical and statical boundary conditions are, respectively, prescribed as follows.

$$u_1(L) = u_2(L) = w(0) = w(L) = w'(L) = 0 \tag{2.4.7}$$

$$M(0) = N_1(0) = N_2(0) = 0 \Rightarrow w''(0) = u_1'(0) = u_2'(0) = 0 \tag{2.4.8}$$

Assembling the governing differential equation 2.4.5, its general and particular solutions, 2.4.4 and 2.4.6, and

the boundary conditions, the eight constants of integration, C_1 to C_8, can be trivially determined through a linearly independent system.

Figures 2.6, 2.7, 2.8 and 2.9 present a parametric study to illustrate the influence of a dimensionless partial composite action parameter αL, proposed by Girhammar [30]. Four different practical values of this parameter are adopted, $\alpha L = 2,\ 5,\ 10,\ 20$.

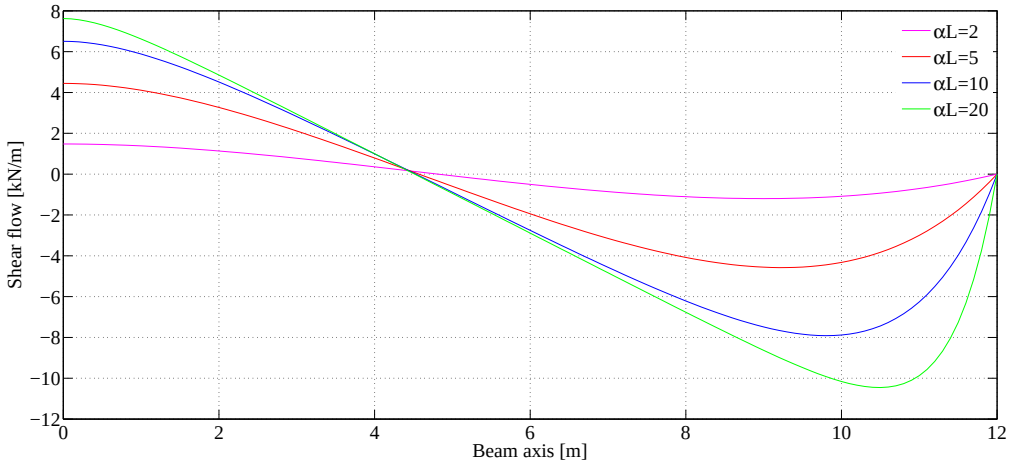

Figure 2.6: Shear flow at the connection interface of the composite beam.

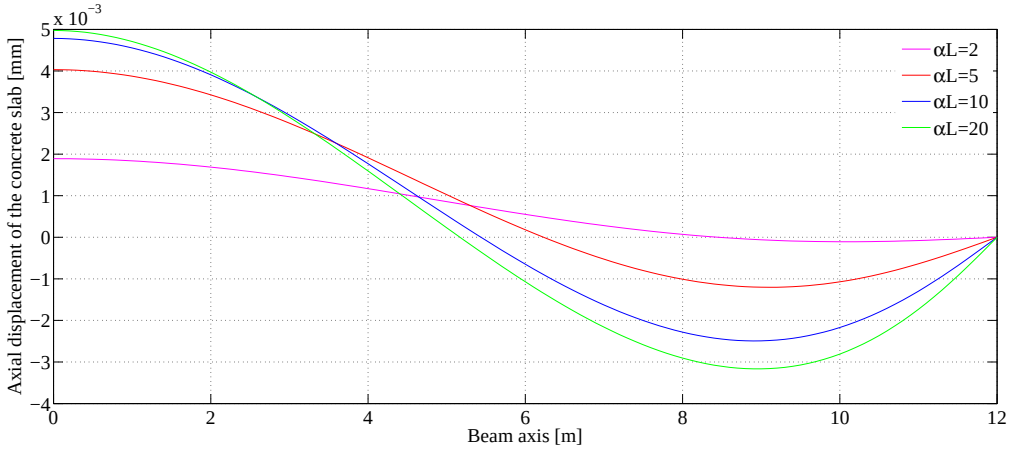

Figure 2.7: Axial displacement of the concrete slab of the composite beam.

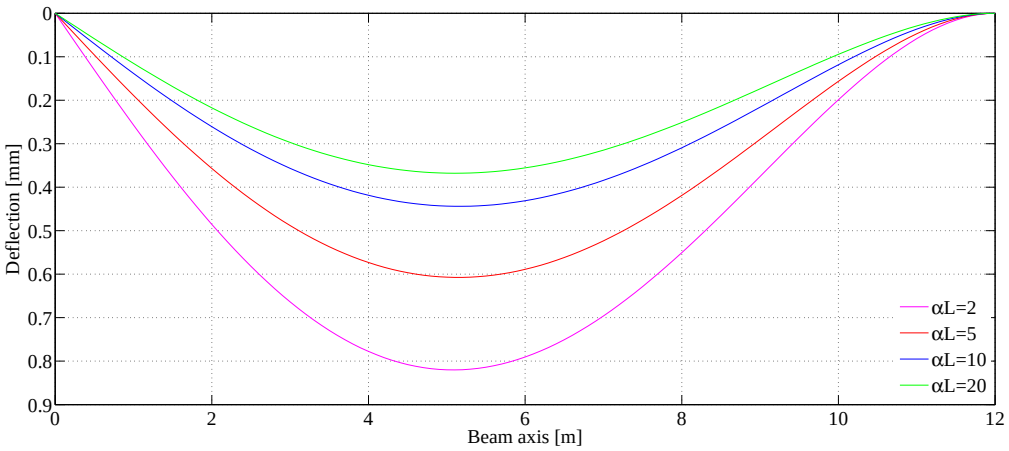

Figure 2.8: Deflection of the composite beam.

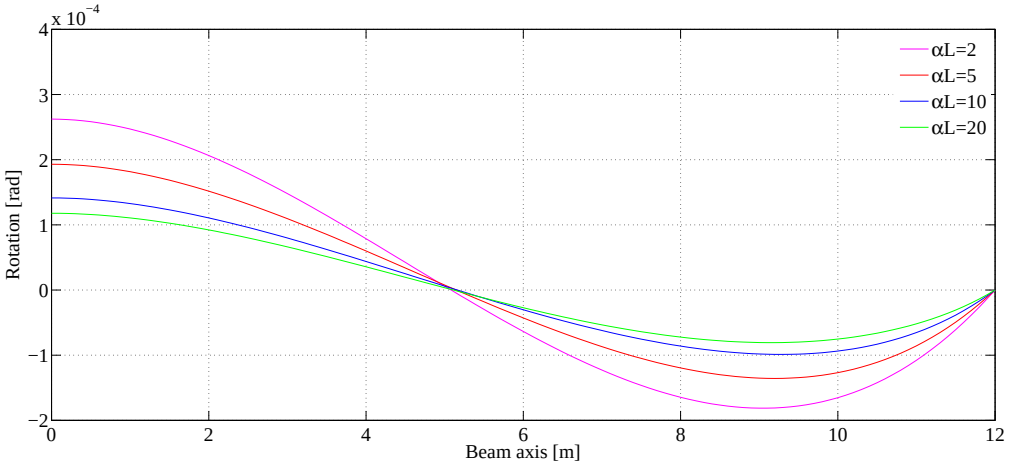

Figure 2.9: Rotation of the composite beam.

Chapter 3

Development of a finite element approximation

3.1 Introduction

The analytical solution described in the previous chapter remains valid when covered by a quite limitative set of conditions. In fact, for some loading and boundary conditions, as well as for physical and geometrical non-linear problems, an analytical solution can be too difficult or even impossible to obtain.

Aside from the connection flexibility discussed in the previous chapter, this work is also focused on the study of the influence of the physical non-linear behaviour of the concrete slab in the global response of a composite beam. In fact, as the constitutive law of the composite beam materials has an approximately linear form just for a quite limited range of loading, the non-linear behaviour of the beam has to be considered in order to perform a serviceability limit state (SLS) analysis of the structure.

Since no analytical solution can be obtained for such a non-linear analysis, an approximate numerical solution based on the principles of the finite element method (FEM) is developed.

Over the last few decades, some numerical models have been formulated concerning the composite beams analysis. Two kinds of numerical models can be found in literature [4]: those formulating the connection devices separately from the steel and concrete elements [28,31]; and those in which the connectors participation is inherently underlying the formulation of the whole composite beam [1,4,16].

In 1993, Aribert *et al* [28] formulated a model with two Euler-Bernoulli beam elements bound together by two uniaxial finite elements, placed at the end nodes, each one with three degrees of freedom (axial dis-

placement of the concrete, axial displacement of the steel and rotation of both steel and concrete).

In 2000 Vieira [4] developed a hybrid formulation approximating not only the displacement field at the boundary but also the stress field over the element's domain. Contrary to the conventional finite elements, which yield a global balanced solution, this hybrid approach allows the equilibrium to be verified at a local level.

Since the redistribution of the axial stress between the concrete slab and the steel beam due to the deformable connection is one of the objectives of this study, it would be preferable to obtain a solution verifying the equilibrium locally [4]. However, this hybrid formulation is beyond the scope of this work.

The following sections of this chapter were written in order to provide a simple explanation of how this particular numerical model is formulated, as well as giving an overview about its computational implementation.

Some illustrative examples were carried out in the linear domain to verify the accuracy of the model. Comparisons with the analytical solution obtained on the previous chapter are presented.

3.2 Finite element formulation

In this section a finite element is proposed for the analysis of composite beams with longitudinal partial interaction,i.e., considering the relative displacement between the steel and the concrete at interface. In view of this, the proposed finite element is formed by coupling two Euler-Bernoulli beam elements through a uniformly distributed spring allowing longitudinal deformation.

Several displacement-based formulations have been developed in order to consider the problem of the longitudinal partial interaction. In 2006 Dall'Asta and Zona [26] have tested three finite elements with 8, 10 and 16 degrees of freedom (dof), comparing their ability to provide accurate results by analysing the non-linear behaviour of a two-span composite beam.

The 8dof element has curvature locking problems, mainly in the hogging region where a high curvature gradient exists, being its use discouraged. Notwithstanding the 10dof and 16dof elements have performed better, both have required significant computational effort.

The governing system of differential equations 2.4.2 along with the boundary conditions 2.3.10 define the

so-called *strong form* of the problem. The strong form is presented by the following equations,

$$E_1 A_1 \frac{d^2 u_1}{dx^2} + \rho_x \left(u_2 - u_1 + h\frac{dw}{dx} \right) = -p_{x1} \tag{2.4.2a}$$

$$E_2 A_2 \frac{d^2 u_2}{dx^2} - \rho_x \left(u_2 - u_1 + h\frac{dw}{dx} \right) = -p_{x2} \tag{2.4.2b}$$

$$-EI_0 \frac{d^4 w}{dx^4} + h\rho_x \left(\frac{du_2}{dx} - \frac{du_1}{dx} + h\frac{d^2 w}{dx^2} \right) = -p_z - \frac{dm}{dx} \tag{2.4.2c}$$

$$u_\alpha(x) - \bar{u}_\alpha = 0 \quad on \quad \Gamma_u \tag{2.3.10a}$$

$$\frac{dw(x)}{dx} + \bar{\theta} = 0 \quad on \quad \Gamma_\theta \tag{2.3.10b}$$

$$w(x) - \bar{w} = 0 \quad on \quad \Gamma_w \tag{2.3.10c}$$

$$N_\alpha(x) - \bar{N}_\alpha = 0 \quad on \quad \Gamma_N \tag{2.3.10d}$$

$$M(x) - \bar{M} = 0 \quad on \quad \Gamma_M \tag{2.3.10e}$$

$$\frac{dM(x)}{dx} + m + hf_x(x) - \bar{V} = 0 \quad on \quad \Gamma_V \tag{2.3.10f}$$

where the bar over some characters denotes a displacement or a force prescribed at the end of the element and Γ represents the different types of physical boundary conditions. It is worth mentioning that either the load or the displacement can be prescribed at a boundary point, but not both.

To formulate the finite elements equations it is necessary to state the differential equations 2.4.1 in an integral form which is referred to as *weak form*. This weak form comes from the application of the method of weighted residuals, an approximation technique for solving differential equations which is the basis for the development of the FEM. In this method, one seeks an approximation solution consisting of a linear combination of interpolation functions to solve differential equations.

The Galerkin method is the subclass of the method of weighted residuals that leads to the element governing equation of the FEM. This method stands out from other methods of weighted residuals because its

weight functions are chosen to be the same as the interpolation functions. More details on this matter can be found in [2, 32].

The resulting weak form is equivalent to the strong form as long as the difference between them, the so-called *residual*, vanishes in an average (or weighted) sense over the element domain. In this context of solid mechanics it is known by the principle of the virtual work, which equals the work produced by the external loads and the internal forces in an arbitrary deformed body.

Considering the governing equation and the boundary conditions associated with the internal axial force multiplied by an arbitrary weight function $\psi(x)$ and integrated over the domain, the weak form of the axial problem on the concrete part is written as follows:

$$\int_0^L \psi \left[E_1 A_1 \frac{d^2 u_1}{dx^2} + \rho_x \left(u_2 - u_1 + h \frac{dw}{dx} \right) + p_{x1} \right] \, dx = 0 \quad \forall \psi \tag{3.2.1a}$$

$$\psi (N_1(x) - \bar{N}_1)|_{\Gamma_N} = 0 \quad \forall \psi \tag{3.2.1b}$$

Integrating by parts the first integral term one is left with:

$$\int_0^L \psi \frac{d}{dx} \left(E_1 A_1 \frac{du_1}{dx} \right) \, dx = \left(\psi E_1 A_1 \frac{du_1}{dx} \right) \Big|_0^L - \int_0^L \frac{d\psi}{dx} E_1 A_1 \frac{du_1}{dx} \, dx \tag{3.2.2}$$

The first term of the right-hand side arises from the *fundamental theorem of calculus*, which states that the integral of a derivative of a function is the function itself. Substituting 3.2.2 into the equation 3.2.1a it follows that:

$$\left(\psi E_1 A_1 \frac{du_1}{dx} \right) \Big|_0^L - \int_0^L \frac{d\psi}{dx} E_1 A_1 \frac{du_1}{dx} \, dx + \int_0^L \psi \rho_x \left(u_2 - u_1 + h \frac{dw}{dx} \right) \, dx + \int_0^L \psi p_{x1} \, dx = 0 \tag{3.2.3}$$

For convenience, the equation 3.2.3 can be rearranged into the following form:

$$\int_0^L \frac{d\psi}{dx} E_1 A_1 \frac{du_1}{dx} \, dx - \int_0^L \psi \rho_x \left(u_2 - u_1 + h \frac{dw}{dx} \right) \, dx = \int_0^L \psi p_{x1} \, dx + \left(\psi \bar{N}_1 \right) \Big|_0^L \tag{3.2.4}$$

A similar procedure can be made to developed the weak form for the axial problem on the steel beam, yielding

the following equation.

$$\int_0^L \frac{d\psi}{dx} E_2 A_2 \frac{du_2}{dx}\, dx + \int_0^L \psi \rho_x \left(u_2 - u_1 + h\frac{dw}{dx} \right) dx = \int_0^L \psi p_{x2}\, dx + \left(\psi \bar{N}_2 \right) \Big|_0^L \tag{3.2.5}$$

Regarding the bending problem on the composite beam, the equilibrium equation 2.4.2c and the static boundary conditions 2.3.10e and 2.3.10f are multiplied by an arbitrary weight function $\psi(x)$, being written as follows:

$$\int_0^L \psi \left[-EI_0 \frac{d^4 w}{dx^4} + h\rho_x \left(\frac{du_2}{dx} - \frac{du_1}{dx} + h\frac{d^2 w}{dx^2} \right) + p_z + \frac{dm}{dx} \right] dx = 0 \quad \forall \psi \tag{3.2.6a}$$

$$\psi (M(x) - \bar{M})|_{\Gamma_M} = 0 \quad \forall \psi \tag{3.2.6b}$$

$$\psi \left(\frac{dM(x)}{dx} + m + h f_x(x) - \bar{V} \right) \Big|_{\Gamma_V} = 0 \quad \forall \psi \tag{3.2.6c}$$

The first integral term is integrated by parts, but this time the procedure must be applied twice, since the differential equation is of fourth-order.

$$\int_0^L \psi \frac{d}{dx} \left(EI_0 \frac{d^3 w}{dx^3} \right) dx = \left(\psi EI_0 \frac{d^3 w}{dx^3} \right) \Big|_0^L - \int_0^L \frac{d\psi}{dx} EI_0 \frac{d^3 w}{dx^3}\, dx \tag{3.2.7}$$

Integrating by parts, once more, the second term of the right-hand side, yields:

$$\int_0^L \frac{d\psi}{dx} \frac{d}{dx} \left(EI_0 \frac{d^2 w}{dx^2} \right) dx = \left(\frac{d\psi}{dx} EI_0 \frac{d^2 w}{dx^2} \right) \Big|_0^L - \int_0^L \frac{d^2\psi}{dx^2} EI_0 \frac{d^2 w}{dx^2}\, dx \tag{3.2.8}$$

Substituting 3.2.8 into 3.2.7 and the result into 3.2.6a the weak form for the bending problem on the composite beam is obtained.

$$\begin{aligned} -\left(\psi EI_0 \frac{d^3 w}{dx^3} \right) \Big|_0^L - \left(\frac{d\psi}{dx} EI_0 \frac{d^2 w}{dx^2} \right) \Big|_0^L - \int_0^L \frac{d^2\psi}{dx^2} EI_0 \frac{d^2 w}{dx^2}\, dx \\ + \int_0^L \psi h \rho_x \left(\frac{du_2}{dx} - \frac{du_1}{dx} + h\frac{d^2 w}{dx^2} \right) dx + \int_0^L \psi \left(p_z + \frac{dm}{dx} \right) dx = 0 \quad \forall \psi \end{aligned} \tag{3.2.9}$$

Equation 3.2.9 is rearranged to be written in the following form:

$$\int_0^L \frac{d^2\psi}{dx^2} EI_0 \frac{d^2w}{dx^2}\ dx - \int_0^L \psi h\rho_x \left(\frac{du_2}{dx} - \frac{du_1}{dx} + h\frac{d^2w}{dx^2}\right)\ dx = \int_0^L \psi \left(p_z + \frac{dm}{dx}\right)\ dx + \left(\psi \bar{V}\right)\Big|_0^L + \left(\frac{d\psi}{dx}\bar{M}\right)\Big|_0^L \quad \forall\psi \quad (3.2.10)$$

After deriving the weak form of the governing equation, it is important to notice that the displacement fields $\mathbf{d}(x)$ constituting the solution of the problem must satisfy the displacement boundary conditions 2.3.10a,2.3.10b,2.3.10c. For this reason these boundary conditions are often called *essential boundary conditions*. On the other hand, the static boundary conditions arise naturally from the weak form, and hence they are called *natural boundary conditions*.

The solution approximating displacement fields is subjected to continuity requirements, that is, it must be continuously differentiable as many times as necessary to do not vanish. By stating the problem in its weak form this continuity requirements are softened, once the order of the derivative affecting the solution is lessened by transferring those derivatives to the weight function. Besides, the integration by parts associated with the development of the weak form leads to a symmetrical stiffness matrix; e.g. the first integral of the left-hand side of equation 3.2.10 is symmetrical regarding both ψ and w.

The three equations representing the weak form can be compactly written in its matrix form as follows:

$$\int_0^{L_e} (\mathscr{D}_s\mathbf{\Psi})^T \mathbf{K}_s \mathscr{D}_s \mathbf{d}_s\ dx = \int_0^{L_e} (\mathscr{H}_s\mathbf{\Psi})^T \mathbf{p}_s\ dx + [(\mathscr{H}_s\mathbf{\Psi})^T \mathbf{Q}_s]_{x=0,L_e} \quad (3.2.11)$$

where $\mathscr{D}_s$ and $\mathscr{H}_s$ are the differential operators presented in the previous chapter; and $\mathbf{Q}_s$ represents the vector of the concentrated loads applied at the ends of the element, being defined as follows:

$$\mathbf{Q}_s^T = \begin{bmatrix} \bar{N}_1 & \bar{N}_2 & \bar{V} & \bar{M} \end{bmatrix}$$

The Galerkin method is a weighted residuals method, usually adopted in displacement-based finite elements formulations. Hence, the approximation functions of the displacement fields are adopted as weight functions. The displacement field, $\mathbf{d}_s$, at an element level, is approximated by a linear combination of interpolation

functions.

$$\mathbf{d}_s \cong \mathbf{\Psi}\mathbf{q}_e \tag{3.2.12}$$

where $\mathbf{q}_e$ is the nodal displacements vector, which represents the weights (or amplitudes) of the interpolation functions and $\mathbf{\Psi}$ is the matrix storing the interpolation functions themselves.

By substituting the approximation of the displacement field into equation 2.4.1 (which is not the exact solution of the governing equation) a residual is obtained:

$$\mathscr{D}_s^* \mathbf{K}_s \mathscr{D}_s \mathbf{\Psi}\mathbf{q}_e - \mathscr{H}_s^* \mathbf{p}_s = \mathbf{R} \neq 0 \tag{3.2.13}$$

To ensure the equilibrium in a global sense, the residual is enforced to be null in a weighted sense over the element domain.

$$\int_0^{L_e} (\mathscr{D}_s \mathbf{\Psi})^T \mathbf{K}_s \mathscr{D}_s \mathbf{\Psi}\mathbf{q}_e \; dx = \int_0^{L_e} (\mathscr{H}_s \mathbf{\Psi})^T \mathbf{p}_s \; dx + [(\mathscr{H}_s \mathbf{\Psi})^T \mathbf{Q}_s]_{x=0,L_e} \tag{3.2.14}$$

Equation 3.2.14 can be compactly written as follows:

$$\mathbf{K}_e \mathbf{q}_e = \mathbf{Q}_e \tag{3.2.15}$$

which corresponds to the well known equation of the displacement method, being $\mathbf{K}_e$ the stiffness matrix of the element.

$$\mathbf{K}_e = \int_0^{L_e} \mathbf{B}^T \mathbf{K}_s \mathbf{B} \; dx \tag{3.2.16}$$

where the matrix $\mathbf{B}$ is given by:

$$\mathbf{B} = \mathscr{D}_s \mathbf{\Psi}$$

Notice that matrix $\mathbf{B}$ relates the vector of the deformation parameters to the vector of the nodal displacements, $\mathbf{q}$. In fact, substituting the approximate solution given by equation 3.2.12 into the compatibility

condition 2.3.7, yields:

$$\mathbf{e}_s \cong \mathscr{D}_s \mathbf{\Psi} \mathbf{q}_e = \mathbf{B}\mathbf{q}_e \tag{3.2.17}$$

The vector $\mathbf{Q}_e$ comprises both terms of the right-hand side of equation 3.2.14. The first term corresponds to the statically equivalent nodal forces,i.e., fictitious forces that associated with an arbitrary deformed shape of structure, produce the same work as the real load distributed along the element; the second term constitutes the concentrated loads applied at the boundary of the element.

$$\mathbf{Q}_e = \int_0^{L_e} (\mathscr{H}_s \mathbf{\Psi})^T \mathbf{p}_s \; dx + [(\mathscr{H}_s \mathbf{\Psi})^T \mathbf{Q}_s]_{x=0,L_e} \tag{3.2.18}$$

The finite element formulated in this section is locally compatible since the interpolations functions are *smooth* enough to ensure all compatibility conditions to be verified at a local level along the element domain. On the other hand, the equilibrium is verified globally by equation 3.2.14,i.e., by weighting the interpolation functions [2]. At the boundary both compatibility and nodal forces are exactly verified since a one-dimension finite element has been adopted and hence the boundary between elements had been reduced to a single point.

3.3 Computer implementation

The numerical model proposed for the analysis of composite beams with flexible connection does not take into account the shear deformation on both the concrete and the steel components. The vertical and rotational deformations at the interface connection are also neglected.

As explained in section 3.2, the exact solution for the displacement field, $\mathbf{d}_s$, at an element level, is approximated by a linear combination of interpolation functions through equation 3.2.12.

The displacement-based finite element considered in the model implementation, approximates the axial and the vertical displacement fields by second and third order polynomials, respectively.

Considering an approximation of the displacement field that adopts for the axial displacement a second-order function plays an important role in the numerical model accuracy. In fact, a linear approximation of this field would generate locking problems associated with the curvature field [26,33]. Further details on this matter can be found in the following section of this chapter.

Two additional internal nodes with axial freedom (u_{1m} and u_{2m}) are required for the second order polynomials, as depicted in figure 3.1.

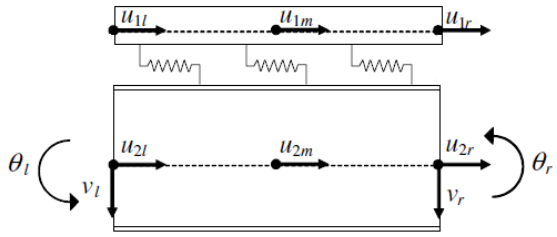

Figure 3.1: Locking-free 10dof element (adapted from [1]).

Therefore, the nodal displacements vector $\mathbf{q}_e$ which represents the weights of the interpolation functions and the matrix $\mathbf{\Psi}$ storing the interpolation functions are given by:

$$\mathbf{q}_e^T = \begin{bmatrix} u_{1l} & u_{2l} & w_l & \theta_l & u_{1r} & u_{2r} & w_r & \theta_r & u_{1m} & u_{2m} \end{bmatrix}$$

$$\mathbf{\Psi} = \begin{bmatrix} \mu_l & \cdot & \cdot & \cdot & \mu_r & \cdot & \cdot & \cdot & \mu_m & \cdot \\ \cdot & \mu_l & \cdot & \cdot & \cdot & \mu_r & \cdot & \cdot & \cdot & \mu_m \\ \cdot & \cdot & \eta_l & \nu_l & \cdot & \cdot & \eta_r & \nu_r & \cdot & \cdot \end{bmatrix}$$

The quadratic polynomials adopted to approximate the longitudinal displacement field are defined as follows:

$$\mu_l = 1 - 3\left(\frac{x}{L_e}\right) + 2\left(\frac{x}{L_e}\right)^2 \qquad (3.3.1a)$$

$$\mu_r = -\left(\frac{x}{L_e}\right) + 2\left(\frac{x}{L_e}\right)^2 \qquad (3.3.1b)$$

$$\mu_m = 4\left(\frac{x}{L_e}\right) - 4\left(\frac{x}{L_e}\right)^2 \qquad (3.3.1c)$$

The Hermitian polynomials adopted to approximate the deflection field for an element are given by:

$$\eta_l = 1 - 3\left(\frac{x}{L_e}\right)^2 + 2\left(\frac{x}{L_e}\right)^3 \qquad (3.3.2a)$$

$$\eta_r = 3\left(\frac{x}{L_e}\right)^2 - 2\left(\frac{x}{L_e}\right)^3 \qquad (3.3.2b)$$

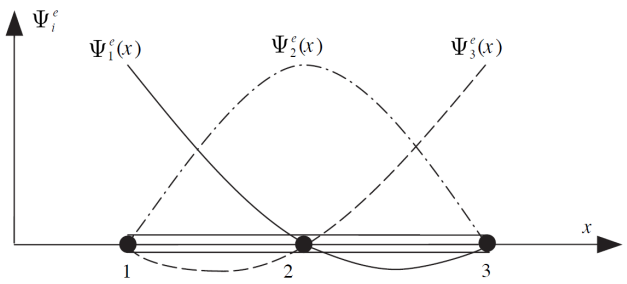

Figure 3.2: Quadratic interpolation functions for a three-node element (adapted from [2])

$$\nu_l = L_e\left(-\left(\frac{x}{L_e}\right)+2\left(\frac{x}{L_e}\right)^2-\left(\frac{x}{L_e}\right)^3\right) \quad (3.3.2c) \qquad \nu_r = L_e\left(\left(\frac{x}{L_e}\right)^2-\left(\frac{x}{L_e}\right)^3\right) \quad (3.3.2d)$$

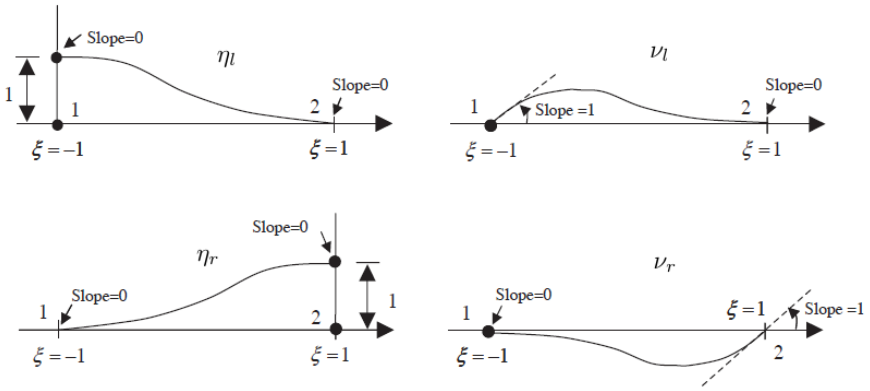

Figure 3.3: Hermitian shape functions for a three-node element.[Adapted from [2]

.

The exact evaluation of the integrals defining the stiffness matrix and the nodal loads in the equation 3.2.15 is not always possible and hence the numerical evaluation of these integral expressions (*numerical integration* or *numerical quadrature*)is adopted.

To apply the *Gauss-Legendre quadrature* or the *Gauss-Lobatto quadrature* one must transform the global coordinate x to a local coordinate ξ, also known as normal or natural coordinate, so that the integral can be evaluated over the interval [-1,1]. The transformation of the coordinate system consists of:

$$x(\xi) = x_a + \frac{L_e}{2}(1+\xi) \quad (3.3.3)$$

in which x_a denotes the global coordinate of the left-end node of the element and L_e represents the element length. The Gauss quadrature formula is given by:

$$\int_{x_a}^{x_b} F(x)\ dx = \int_{-1}^{1} \hat{F}(\xi)\ d\xi \cong \sum_{i=1}^{N} \hat{F}(\xi_i) w_i \tag{3.3.4}$$

in which ξ_i represents the quadrature points, w_i are the quadrature weights and $\hat{F}$ is the transformed integrand given by:

$$\hat{F}(\xi) = F(x(\xi))J(\xi), \quad dx = Jd\xi \tag{3.3.5}$$

where J is the Jacobian of the transformation between x and ξ. The Gauss-Legendre quadrature is the most commonly used because it requires fewer quadrature points to obtain the same accuracy, in comparison with other numerical integration methods. To integrate exactly a polynomial of degree p one employs $2n-1$ Gauss points [32].

Thus, the polynomials presented in equations 3.3.1 and 3.3.2, which constitute the approximation matrix Ψ are implemented considering the transformation 3.3.5, being written as:

$$\mu_l = \frac{1}{2}\xi(\xi-1) \qquad (3.3.6a) \qquad \mu_r = \frac{1}{2}\xi(\xi+1) \qquad (3.3.6b) \qquad \mu_m = 1-\xi^2 \qquad (3.3.6c)$$

$$\eta_l = 1 - \frac{1}{4}(\xi+1)^2(2-\xi) \qquad (3.3.7a) \qquad \eta_r = \frac{1}{4}(\xi+1)^2(2-\xi) \quad (3.3.7b)$$

$$\nu_l = -\frac{1}{8}L_e(\xi+1)(1-\xi)^2 \qquad (3.3.7c) \qquad \nu_r = \frac{1}{8}L_e(\xi+1)^2(1-\xi) \quad (3.3.7d)$$

3.3.1 Curvature locking

The 10dof element presented in section 3.2 was meant to avoid curvature locking phenomena occuring for high stiffness values of the interface connection [26, 27, 33]. An algebraic demonstration of this phenomenon

is provided in this section.

Considering the axial and vertical displacement fields approximated, respectively, by a third and first order polynomials(which is the case of the 10dof element) it follows that:

$$w = \gamma_3\xi^3 + \gamma_2\xi^2 + \gamma_1\xi + \gamma_0 \tag{3.3.8a}$$

$$u_\alpha = \bar{\gamma}_{\alpha 1}\xi + \bar{\gamma}_{\alpha 0} \tag{3.3.8b}$$

with $\alpha = 1,\ 2$ for the concrete and steel elements, respectively; and

$$\gamma_3 = \frac{1}{4}w_l - \frac{1}{4}w_r - \frac{1}{8}\theta_l - \frac{1}{8}\theta_r \tag{3.3.9a}$$

$$\gamma_2 = \frac{1}{8}L_e\theta_l - \frac{1}{8}L_e\theta_r \tag{3.3.9b}$$

$$\gamma_1 = -\frac{3}{4}w_l + \frac{3}{4}w_r + \frac{1}{8}L_e\theta_l + \frac{1}{8}L_e\theta_r \tag{3.3.9c}$$

$$\gamma_0 = w_l - \frac{1}{8}L_e\theta_l + \frac{1}{8}L_e\theta_r \tag{3.3.9d}$$

$$\bar{\gamma}_{\alpha 1} = \frac{1}{2}u_{\alpha l} - \frac{1}{2}u_{\alpha r} \tag{3.3.9e}$$

$$\bar{\gamma}_{\alpha 0} = \frac{1}{2}u_{\alpha l} + \frac{1}{2}u_{\alpha r} \tag{3.3.9f}$$

$$\xi = \frac{2x}{L_e} - 1 \tag{3.3.9g}$$

where L_e represents the finite element length, and $w_l,\ w_r,\ \theta_l,\ \theta_r,\ u_l$ and u_r are the nodal displacements which weigh the shape functions, that is to say the vertical displacements, rotations and axial displacements

at $\xi = -1,\ 1$.

The longitudinal slip can be re-stated based on the notation introduced in equations 3.3.9 as:

$$\delta = u_2 - u_1 + h\frac{dw}{dx} = \phi_2\xi^2 + \phi_1\xi + \phi_0 \tag{3.3.10}$$

where

$$\phi_2 = 3h\gamma_3 \tag{3.3.11a}$$

$$\phi_1 = \bar{\gamma}_{21} - \bar{\gamma}_{11} + 2h\gamma_2 \tag{3.3.11b}$$

$$\phi_0 = \bar{\gamma}_{20} - \bar{\gamma}_{10} + h\gamma_1 \tag{3.3.11c}$$

In the limit case where the interface connection stiffness tends to infinity, the longitudinal relative displacement becomes null.

$$\lim_{\rho\to\infty} \delta = 0 \tag{3.3.12}$$

This condition implies that all constants present in equation 3.3.10 must vanish.

$$\phi_2 = \phi_1 = \phi_0 = 0 \tag{3.3.13}$$

The fact of ϕ_2 being null induces a kinematic restraint on the vertical displacement field where the third-order terms, affected by γ_3, disappear. Hence, the cubic polynomial, in the equation 3.3.8a, is reduced down to a parabolic one.

$$w = \gamma_2\xi^2 + \gamma_1\xi + \gamma_0 \tag{3.3.14}$$

Thus, the finite element would be able to produce only constant curvature along its length. This situation occurs every time the polynomials contributing for the evaluation of longitudinal slip are of different or-

ders [26, 27, 33].

3.4 Applications

3.4.1 Introduction

The proposed finite element has been developed under MATLAB environment. A few examples have been performed and some conclusions with respect to the influence of the interface connection stiffness have been drawn.

The numerical solutions obtained through the developed program are compared with the analytical solutions, defined in section 2.4, to evaluate the effectiveness of the finite element formulated. To this end, three examples have been considered: a simply supported beam subjected to a uniformly distributed load and a concentrated load applied at mid-span, and a continuous beam of two equal spans subjected to a uniformly distributed load. Both simply supported beams are 12 m long whereas the continuous beam is 24m long. Their cross sections are formed by a concrete slab of class C30/37 and dimension 3000 mm x 150 mm, and by a hot rolled steel beam IPE500 of grade S275.

Regarding the interface connection, four different solutions were adopted in order to evaluate the influence of the connection stiffness in composite beams behaviour. Two rows of connectors with 19 mm of diameter and a length of 100 mm were considered to be uniformly distributed with longitudinal spacings of 7000 mm, 1150 mm, 285 mm and 70 mm.

According to the shear connectors' constitutive law proposed by Johnson [34](cited by [4, 7, 28]) based on experimental results, a ρ modulus (relating shear force and displacement) of 150 kN/mm has been adopted. This value derives from the secant stiffness corresponding to 50% of the ultimate load a shear connector.

In 1993, Girhammar [30] introduced a dimensionless parameter αL representing the composite action, where L is the beam length and α is given by:

$$\alpha^2 = \rho_x \left(\frac{EA_0}{E_1 A_1 E_2 A_2} + \frac{h^2}{EI_0} \right)$$

For a single row of shear connectors with 19 mm of diameter and a length of 100 mm with a longitudinal spacing of 150 mm, an approximate secant stiffness of 10^6 kN/m^2 is estimated. Rendering this value into the

Girhammar's stiffness parameter for a 12 m long beam it corresponds to $\alpha L = 14.8$, which is consistent with the ranges proposed by Girhammar [30], $1 < \alpha L < 15$ and Ranzi [1], $1 < \alpha L < 20$.

A parametric study is herein performed for values of $\alpha L = 2,\ 5,\ 10$ and 20 (which correspond respectively to the longitudinal spacings of 7000 mm, 1150 mm, 285 mm and 70 mm) to investigate the influence of the shear connection stiffness on the overall structural response.

3.4.2 Simply supported beam

A simply supported composite beam with a 12 m span is subjected to a uniform distributed load of 1 kN/m, as represented in figure 3.4. A symmetry simplification is adopted so that a mesh with a single finite element can be used to solve the problem.

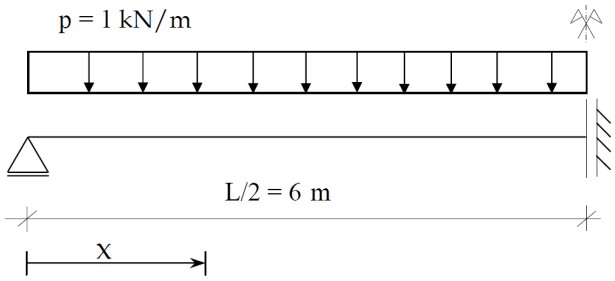

Figure 3.4: Simply supported beam (model with symmetry simplification) subjected to a uniform distributed load.

The deformed shapes of the composite beam, obtained analytically for different values of the connection stiffness parameter are presented in figure 3.5. The amplitude of the vertical displacements increases for lower values of the shear connection stiffness. It is worth noting that in the case of the lowest stiffness value, $\alpha L = 2$, the mid-span deflection is more than 50 % superior to the case in which the stiffness parameter is the highest one, $\alpha L = 20$.

The mid-span deflection of the composite beam for different values of the interface connection stiffness obtained numerically with the developed model considering a mesh of four finite element is represented in figure 3.6. An analytical solution is also presented to be compared with the numerical one, being verified an excellent agreement.

The analytical solution of the shear flow along the composite beam resisted by the interface connection as its stiffness takes four different values is represented in figure 3.7. It can be verified that, depending on the connection stiffness, the shear flow at the end cross section can reach nearly 50% of the value which would be attained in the case of an infinitely high connection stiffness.

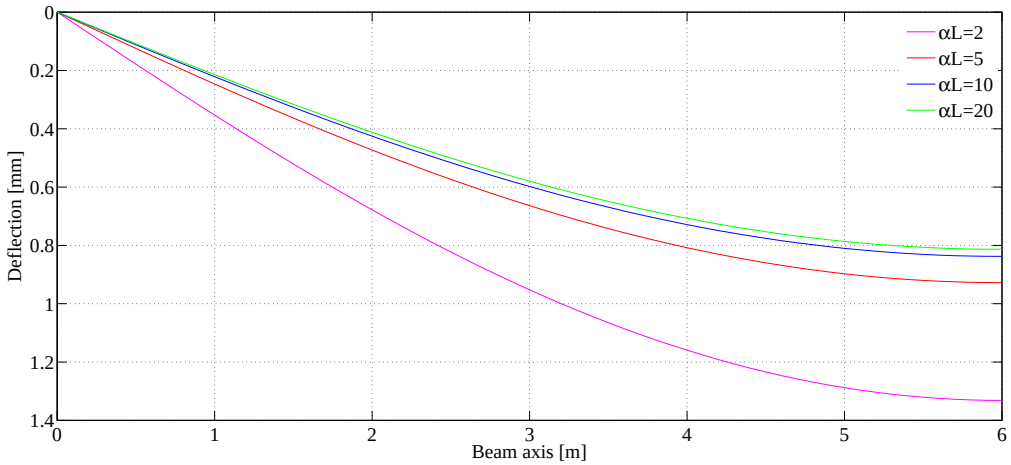

Figure 3.5: Vertical displacement of the composite beam (analytical solution).

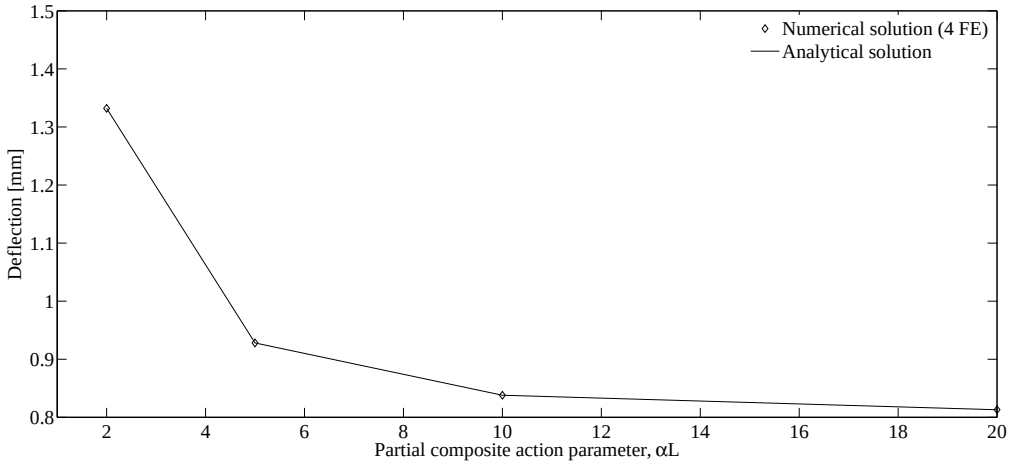

Figure 3.6: Mid-span deflection of the composite beam (numerical solution/analytical solution).

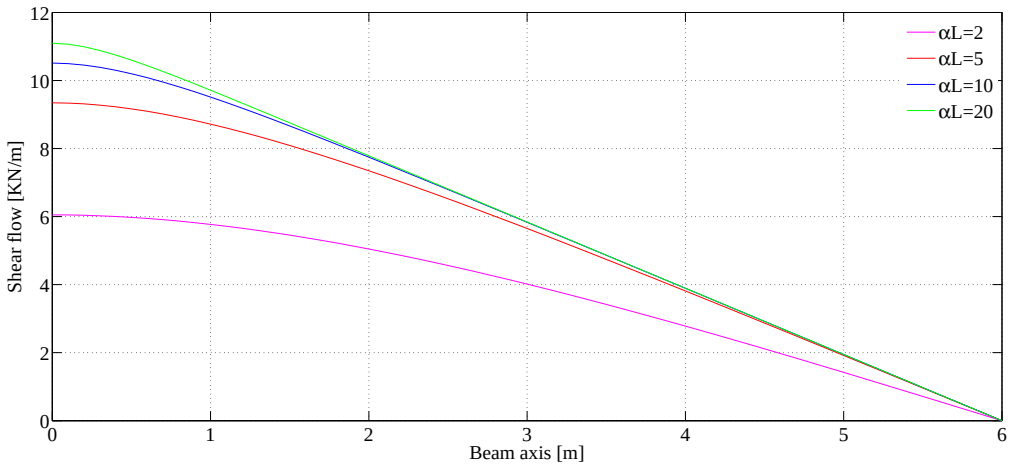

Figure 3.7: Shear flow distribution along the steel-concrete interface (analytical solution).

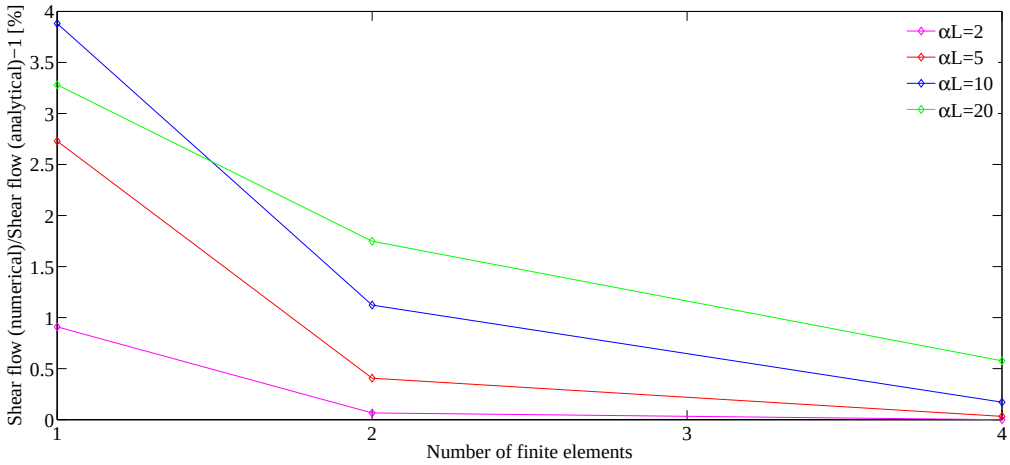

Figure 3.8: Relative error in the approximation of the shear flow at the end support section of the composite beam (numerical solution/analytical solution).

The ability of the finite element model to approximate the shear flow at the end cross section of the composite beam with different discretisations is represented in figure 3.8. The approximation error tends to zero as the mesh is refined, though for high connection rigidities a more refined mesh is required to significantly decrease the error. Nevertheless, even with just one finite element, the maximum error is less than 4%.

The axial stress distribution at the mid-span composite cross section, determined analytically is represented in figure 3.9. It can be verified that the part of the composite section most affected by the connection deformation is the top flange of the steel girder, in which the axial stress variation, owing to a decrease of the connection stiffness from $\alpha L = 5$ to $\alpha L = 2$, exceeds 700%. Conversely, the steel bottom flange's maximum stress variation, even assuming a wider range of the connection stiffness, $2 < \alpha L < 20$, does not surpass 11%.

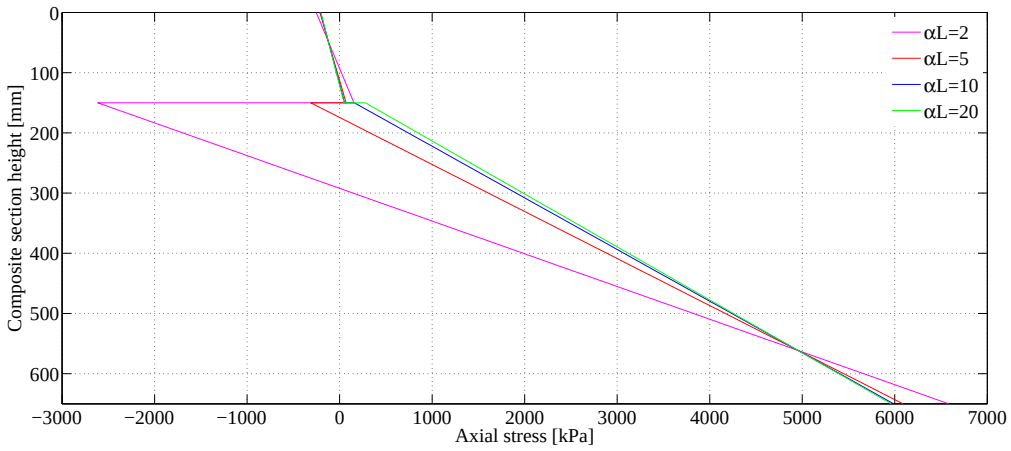

Figure 3.9: Axial stress diagram at the mid-span composite section (analytical solution).

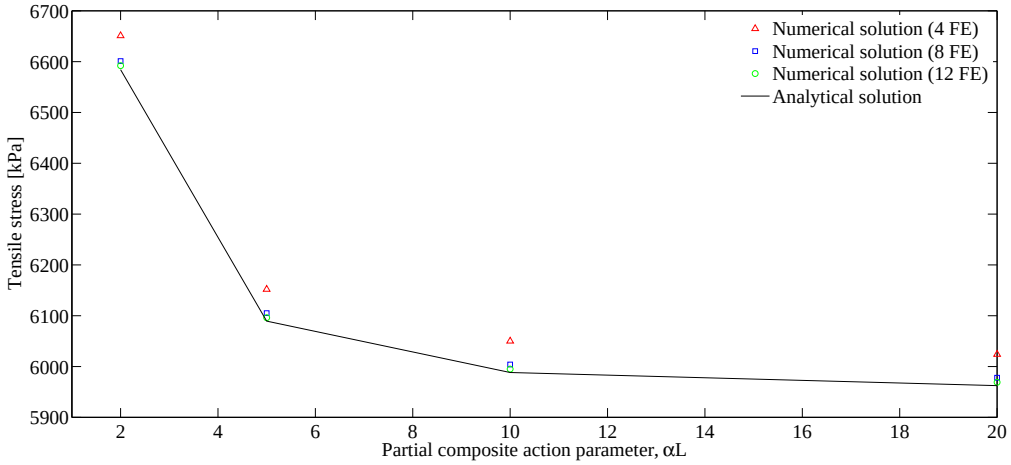

Figure 3.10: Maximum tensile stress at the mid-span composite section (numerical solution/analytical solution).

The maximum tensile stress at the mid-span composite section, located at the bottom fibre of the steel beam, is represented in figure 3.10 as a function of the connection stiffness. A comparison between the analytical and the numerical solutions obtained with four, eight and twelve finite elements is made. Since the results obtained with four finite elements have not proven to be accurate enough, two other meshes were tested. Sufficiently good results are obtained for a twelve-element mesh.

The longitudinal distribution of the axial stress in the concrete slab's top and bottom fibres is plotted in figure 3.11. The numerical results obtained with a uniform mesh of four finite elements are superimposed to the analytical results in order to check the accuracy of this finite element approximation. A dimensionless connection stiffness value of 20 was considered.

The distribution of the shear flow along the beam axis, comparing the results obtained from the analytical

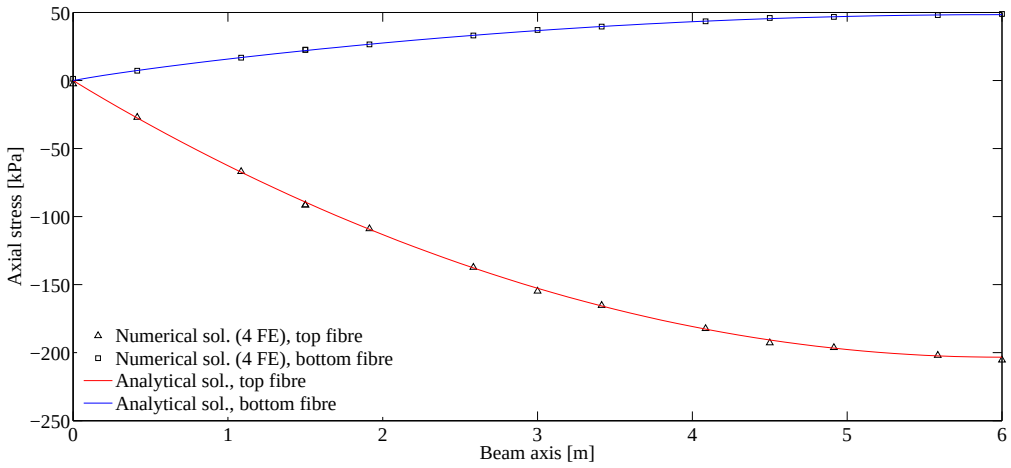

Figure 3.11: Axial stress in the concrete slab.

and numerical models, is represented in figure 3.12. The results of a uniform mesh with four finite elements demonstrate a higher accuracy of the numerical model.

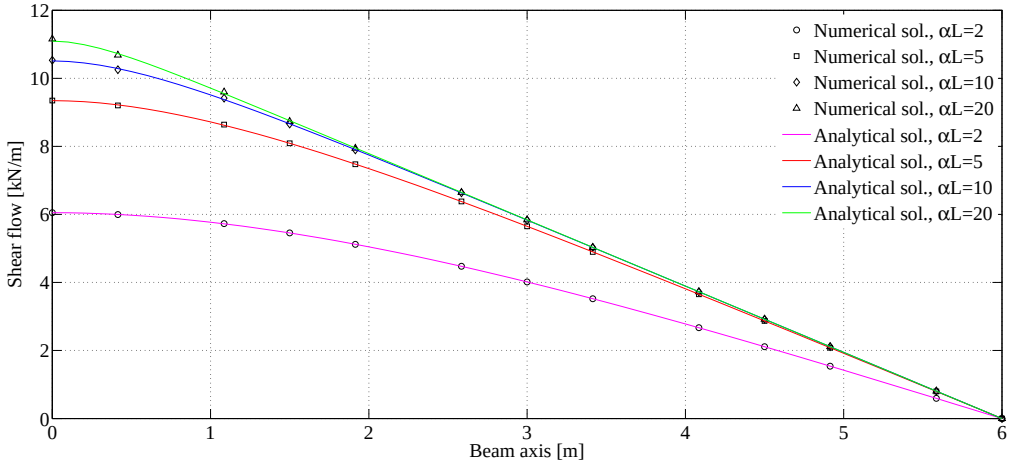

Figure 3.12: Shear flow distribution along the steel-concrete interface (numerical solution with 4 FE/analytical solution).

The composite beam is now subjected to a concentrated load of 1 kN applied at the mid-span, as depicted in figure 3.13.

The vertical displacements of the composite beam are represented in figure 3.14. Once more, the deflections increase for lower values of the connection stiffness. For $\alpha L = 2$ the vertical displacement at the mid-span is more than 60% superior to the case in which $\alpha L = 20$. A significant decrease in the mid-span deflection can be noticed when this stiffness parameter is modified from 2 to 5. Analytical and numerical results of the mid-

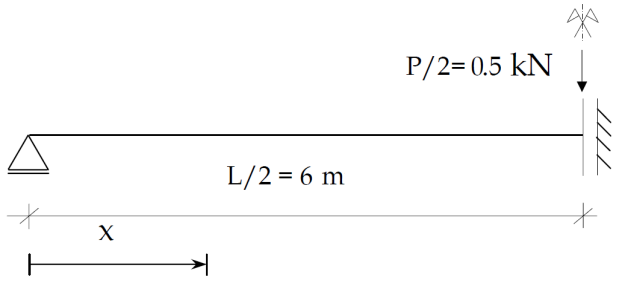

Figure 3.13: Simply supported beam (model with symmetry simplification) subjected to a point load.

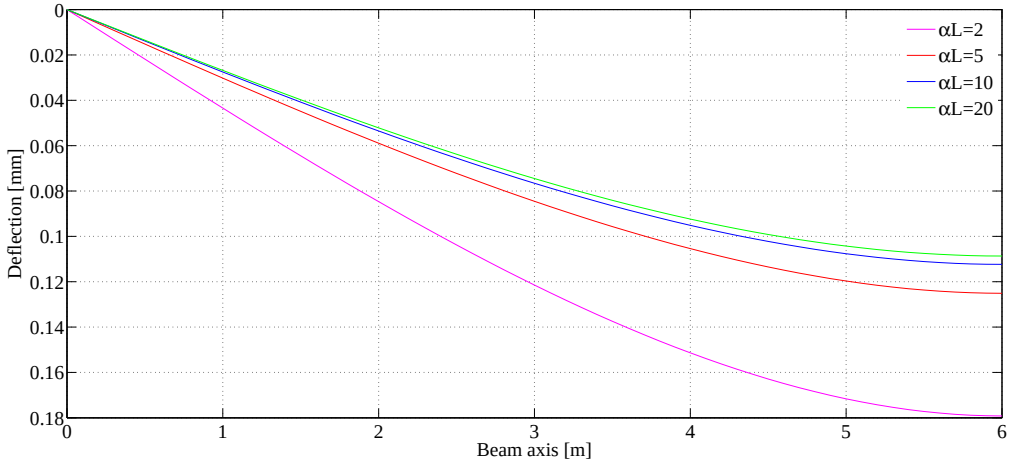

Figure 3.14: Vertical displacement of the composite beam (analytical solution).

span deflection as a function of the composite action parameter are shown in figure 3.15. The two solutions are perfectly superimposed, demonstrating the good accuracy of the numerical model for the evaluation of displacements.

The effect of the connection flexibility in the distribution of the shear force at the steel-concrete interface is plotted in figure 3.16, being significant its influence on the load application region.

The convergence of the numerical model regarding the evaluation of the shear flow at the end section as the finite element mesh is refined, is presented in figure 3.17. In fact, the error is significantly reduced when two finite elements are adopted instead of a single one, being nearly null when four elements are employed. The influence of the connection flexibility is much higher for the coarser meshes.

The distribution of the axial stress along the composite section's height is represented in figure 3.18 for different values of the connection stiffness parameter. A comparison between analytical and numerical results of the maximum tensile stress at the mid-span is presented in figure 3.19. The values coming from the eight-element model proved to be accurate enough.

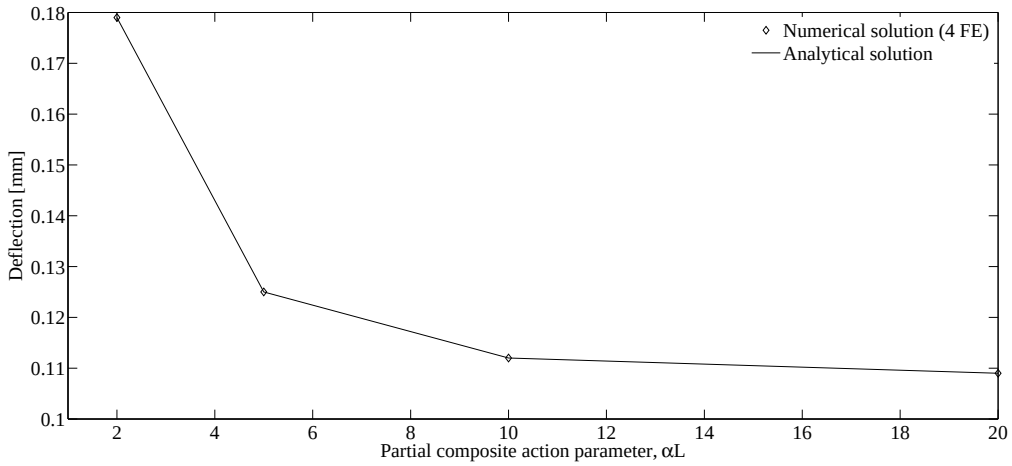

Figure 3.15: Mid-span deflection of the composite beam (numerical solution/analytical solution).

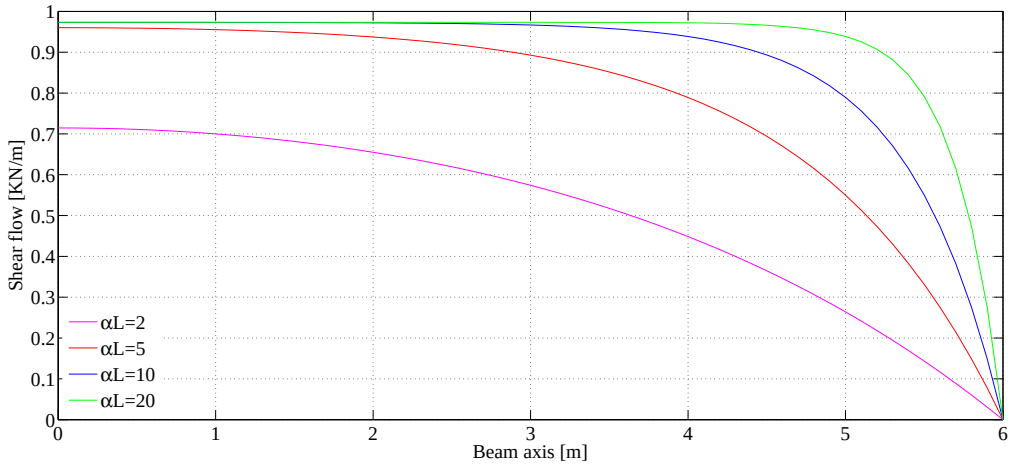

Figure 3.16: Shear flow distribution along the steel-concrete interface (analytical solution).

The variance of the axial stress on the top and the bottom fibres of the concrete slab, determined numerically with a uniform mesh of four elements, is compared with the analytical solution in figure 3.20. Though the sufficient accuracy of the numerical model, some unbalanced points at the boundary between the third and fourth elements can be noticed. This is due to the fact of the equilibrium being imposed globally in a weighted sense, not being verified at a local level.

The shear flow distribution along the beam axis is determined analytically and numerically through a uniform four-element mesh, being a comparison presented in figure 3.21. For low values of the connection stiffness the numerical and analytical results are in good agreement. However, when this parameter increases, a deviation between the numerical and the analytical solution arises. This lack of precision could be overcome by a mesh refinement or an enrichment of the approximation polynomials.

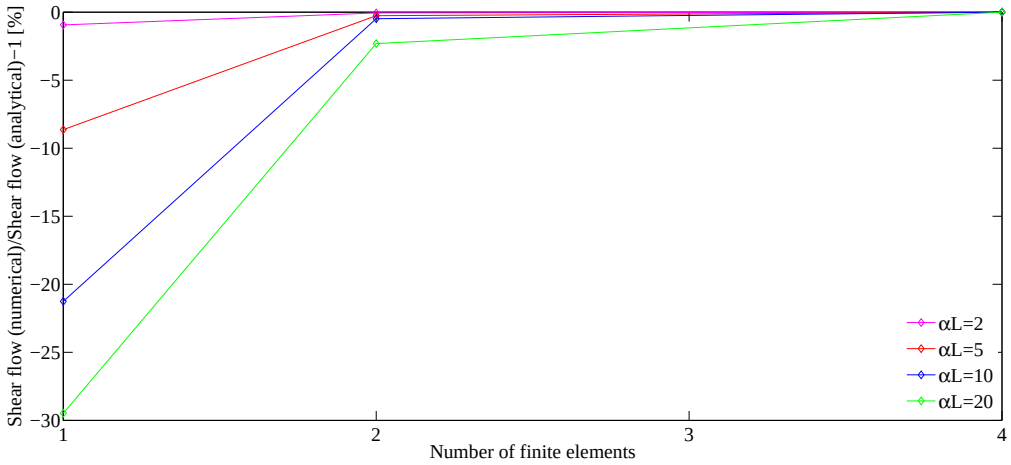

Figure 3.17: Relative error in the approximation of the shear flow at the end support section of the composite beam (numerical solution/analytical solution).

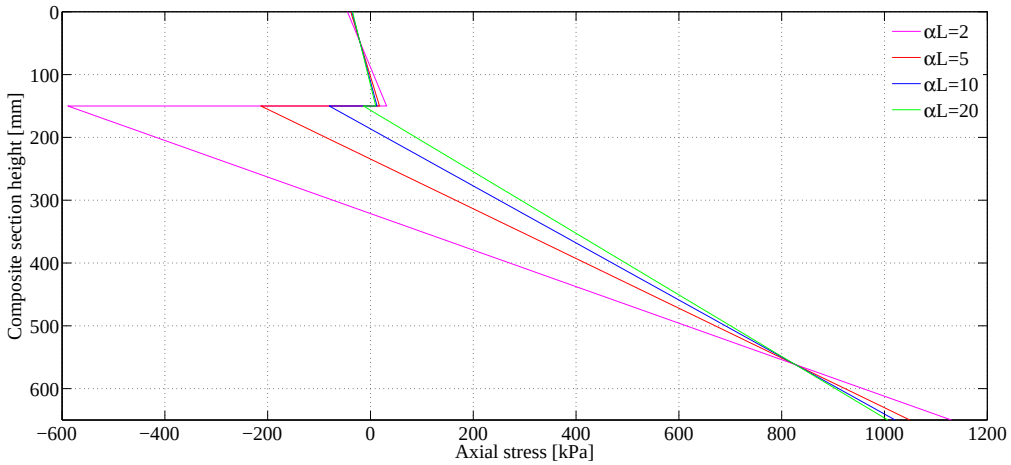

Figure 3.18: Axial stress diagram at the mid-span composite section (analytical solution).

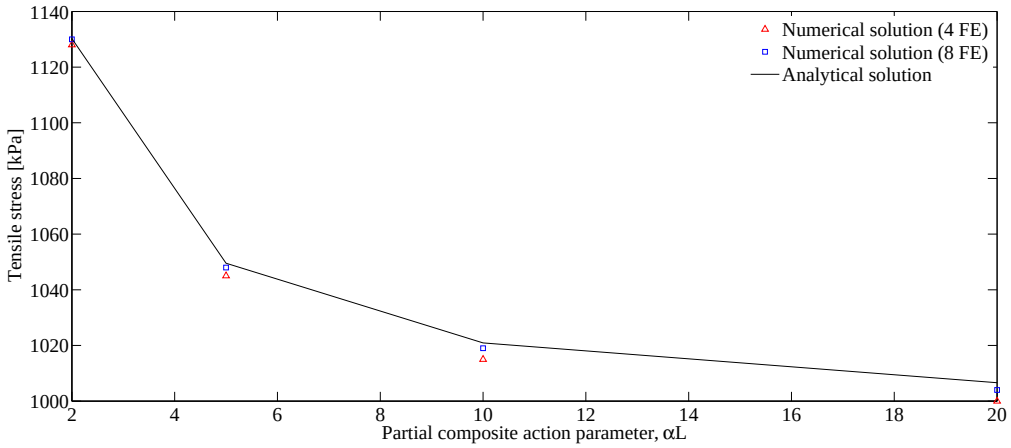

Figure 3.19: Maximum tensile stress at the mid-span composite section (numerical solution/analytical solution).

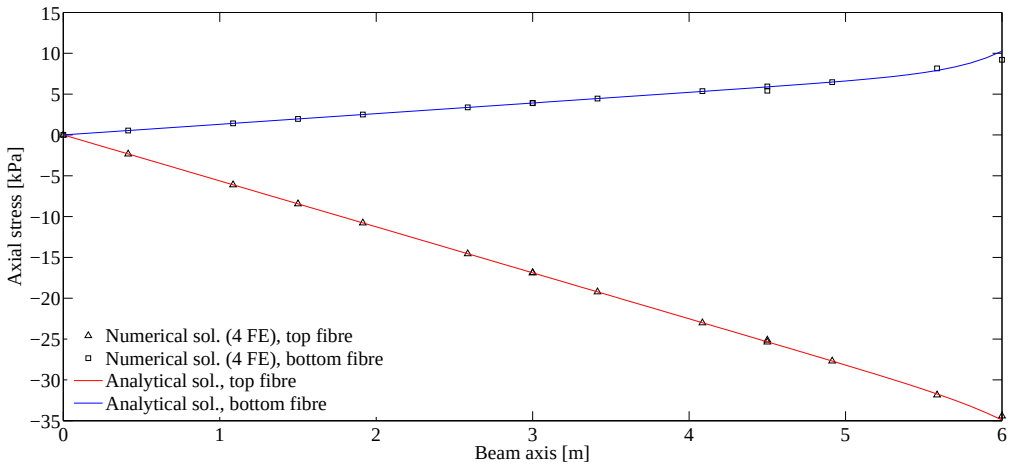

Figure 3.20: Axial stress in the concrete slab.

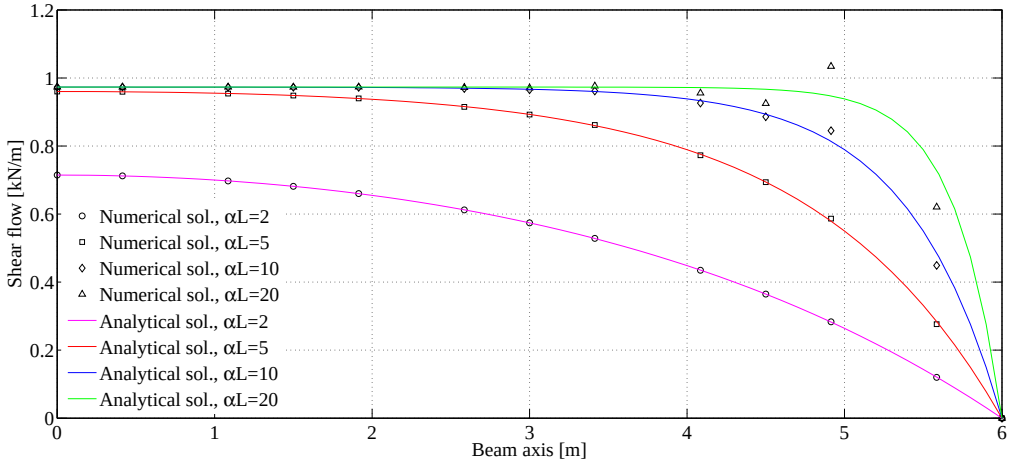

Figure 3.21: Shear flow distribution along the steel-concrete interface (numerical solution with 4 FE/analytical solution).

3.4.3 Two-span continuous beam

The third example consists of a two-span continuous beam subjected to a unitary distributed load, as represented in figure 3.22.

Through the analysis of figure 3.23 representing the analytical solution of vertical displacements, one concludes that by enhancing the connection flexibility greater deflections are obtained. In fact, the mid-span deflection corresponding to the highest connection stiffness value ($\alpha L = 20$) is less than 50% of the mid-span deflection obtained for the lowest connection stiffness ($\alpha L = 2$). The comparison between analytical and numerical solutions presented in figure 3.24 proves, once more, the reliability of this finite element model to

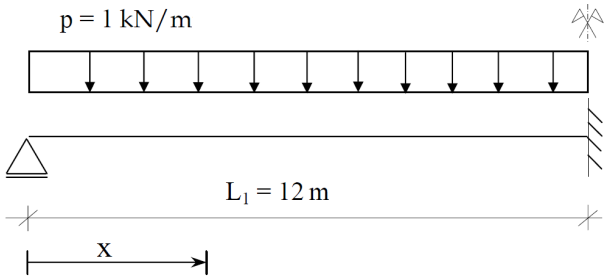

Figure 3.22: Continuous beam with two equal spans (model with symmetry simplification) subjected to a uniform distributed load.

evaluate displacements.

The longitudinal distribution of shear flow over the steel-concrete interface is reported in figure 3.25. The end support and the hogging regions are those where the influence of the connection stiffness is evident. The variation of shear flow along the beam length is flattened as the connection stiffness decreases. Figure 3.26 reveals a large error when a mesh with a single element is utilised to evaluate the shear flow at the end support section. However the high convergence rate of this method renders the error acceptable when four finite elements are used in this approximation.

The vertical distribution of axial stress at the continuity support section is presented in figure 3.27. The region of the composite section that the connection flexibility affects most is the top flange of the steel beam, where the axial stress ranges from 1 MPa to 7 MPa.

The values of the maximum compression stress of the composite section located over the continuity support

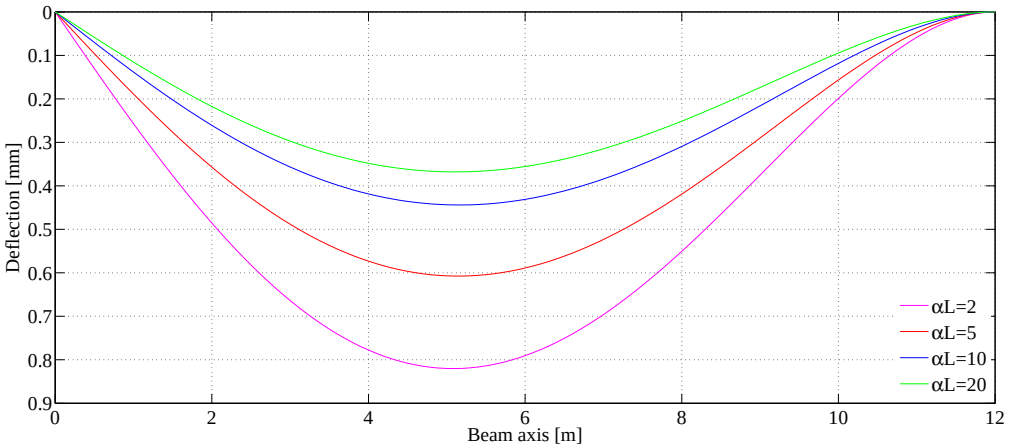

Figure 3.23: Vertical displacement of the composite beam (analytical solution).

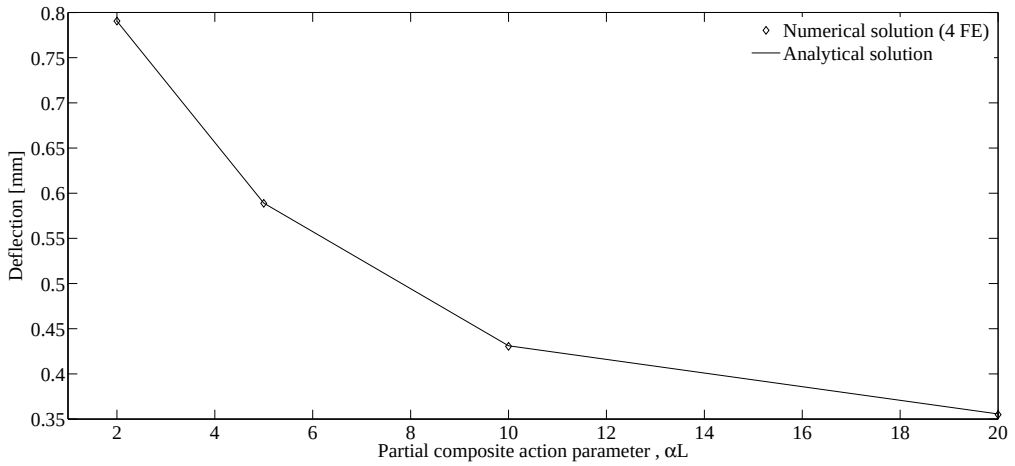

Figure 3.24: Mid-span deflection of the composite beam (numerical solution/analytical solution).

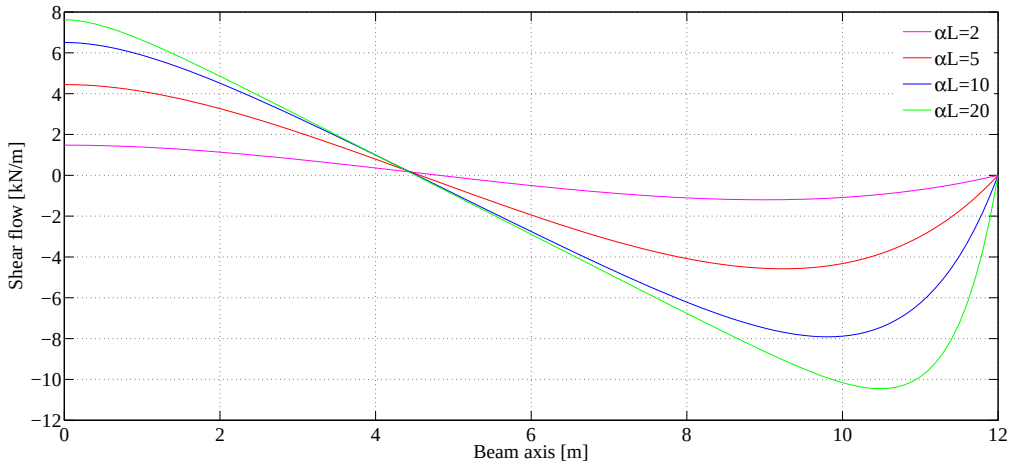

Figure 3.25: Shear flow distribution along the steel-concrete interface (analytical solution).

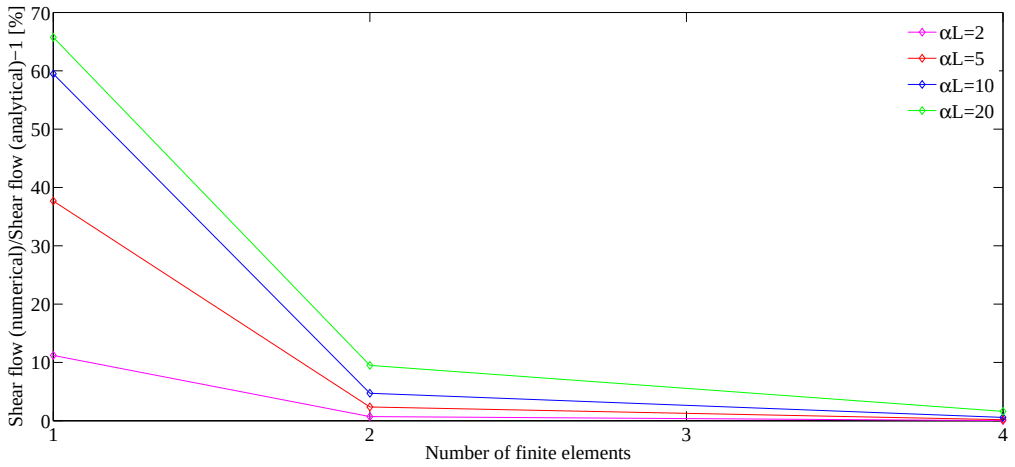

Figure 3.26: Relative error in the approximation of the shear flow at the end support section of the composite beam (numerical solution/analytical solution).

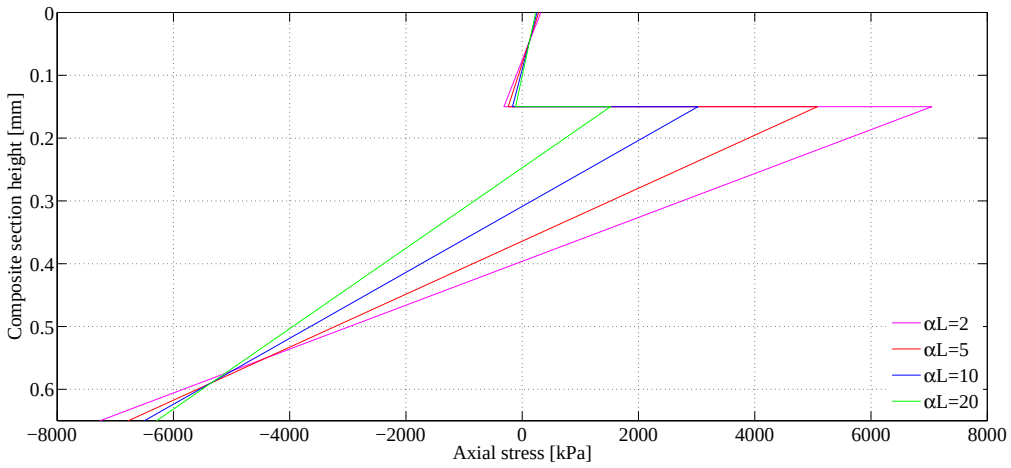

Figure 3.27: Axial stress diagram at the continuity support composite section (analytical solution).

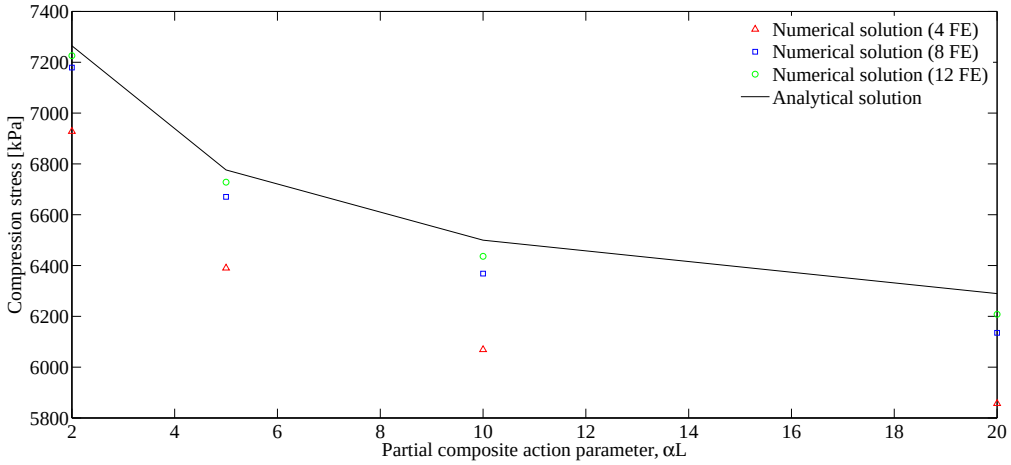

Figure 3.28: Maximum compression stress at the continuity support composite section (numerical solution/analytical solution).

are presented in figure 3.28. Different levels of discretisation have been utilised to evaluate the accuracy of the model. The results obtained for meshes with four, eight and twelve elements, are compared with the analytical solution. The error obtained with the finest mesh appears to be negligible.

The numerical model with a uniform four-element mesh provides reliable results in what concerns the longitudinal distribution of the axial stress of the concrete slab's top and bottom fibres. The good agreement between numerical and analytical solutions can be seen in figure 3.29.

A comparison between the numerical solution, considering four finite elements, and the analytical solution of the longitudinal distribution of the shear flow at the connection interface is plotted in figure 3.30. As shown in the example of a concentrated load acting on a simply supported composite beam, the numerical solution does not perform a good approximation for higher values of the connection stiffness on the hogging region,

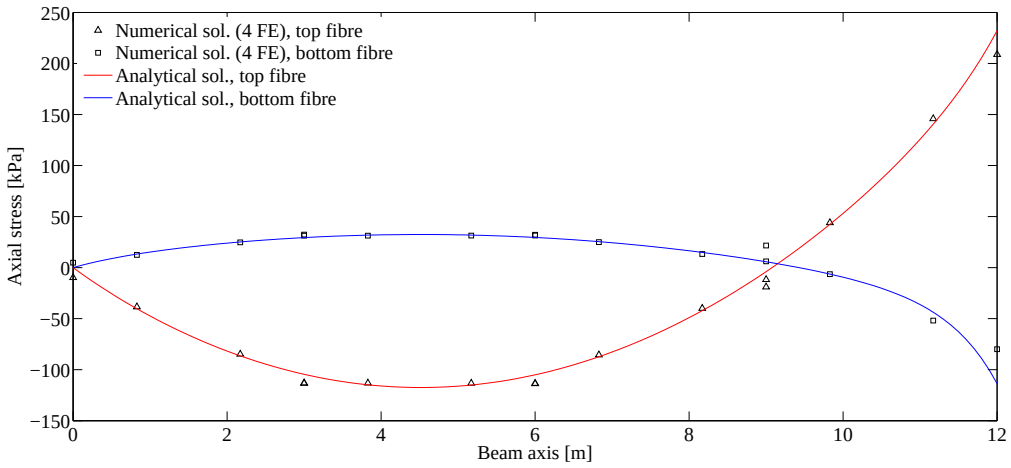

Figure 3.29: Axial stress in the concrete slab.

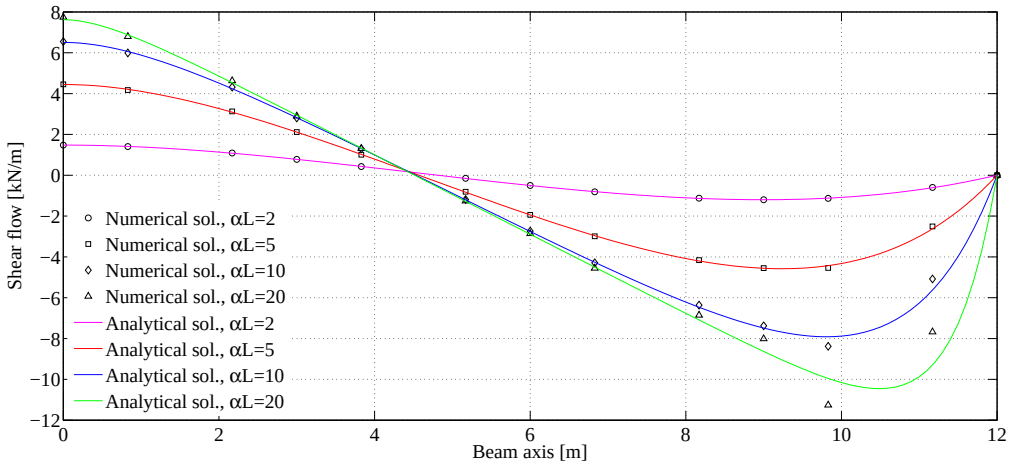

Figure 3.30: Shear flow distribution along the steel-concrete interface (numerical solution with 4 FE/analytical solution).

where the shear flow gradient is significant.

3.4.4 Concluding remarks

The illustrative examples performed in this section have proven that the proposed 10dof locking-free finite element performs well in the approximation of both displacements and stresses, even with a few number of finite elements. Analytical solutions have been developed for each case to be adopted as benchmarks.

Some difficulties were detected in the approximation of the shear flow near the application of concentrated loads, where the tangent of the shear flow is too steep to be "followed" by the quadratic approximations adopted. This obstacle could be mitigated either by enhancing the mesh discretisation [4, 18, 25] or by in-

creasing the order of the polynomials employed [15, 20].

Hence, it can be concluded that the proposed model constitutes a reliable tool in the linear analysis of composite beams with partial interaction for practical values of the interface connection stiffness, i.e., αL ranging from 1 to 20 [1].

Chapter 4

Analysis of composite beams considering the non-linear behaviour of the concrete slab

4.1 Introduction

A non-linear analysis method is introduced in this chapter for the purpose of studying the influence of concrete cracking in the global response of steel-concrete composite beams. In fact, in addition to the flexibility of the shear connection, which has already been taken into account, also the concrete cracking causes a redistribution of the axial stresses between the concrete slab and the steel beam.

Therefore, the structural steel and the shear connection are assumed to remain in linear regimes, whereas a non-linear constitutive law is adopted for the reinforced concrete, including the branch representing the *strain-softening*.

Some adjustments must be made on the linear formulation presented in chapter 2. In fact, the stiffness matrix's components are no longer explicitly defined since they become non-linear function of the composite cross section deformation. Hence, a numerical procedure is implemented in order to solve the problem.

On the following sections, the constitutive law describing the structural concrete's non-linear behaviour is presented as well as the numerical method adopted to perform the corresponding non-linear analysis.

Finally, a two-span continuous beam subjected to distributed and concentrated loads is analysed through the

proposed model, considering either the strain-softening branch or neglecting the concrete under tension. The results obtained from the model are compared with the solution obtained according EN 1994-1-1 and with the linear model, in which no moment redistribution occurs.

4.2 Constitutive law for structural concrete

A non-linear constitutive law for structural concrete is implemented to evaluate the moment redistribution on the hogging region of continuous beams. For this purpose two different constitutive laws are adopted: (i) one that considers the tensile strength to be null; (ii) and other that considers the limited tensile strength preceding the occurrence of cracks (f_{ctm}) and the *strain-softening* effect, i.e., the declining branch of the stress-strain curve.

Concrete under compression is assumed to behave in a linear-elastic manner. The focus of this study is on the serviceability limit state, therefore no extra accuracy would come from the consideration of the actual non-linear behaviour of the concrete under compression.

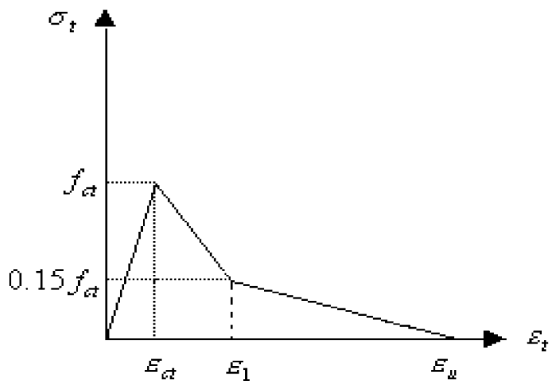

Figure 4.1: Stress-strain of concrete under tension (adapted from [3]).

Prior to cracking, the relation between tensile stress, f_{ct}, and tensile strain, ε_{ct}, is considered to be linear-elastic and the corresponding Young's modulus is equal to E_c. When the tensile stress is exceeded the constitutive law follow a bi-linear strain-softening branch, as depicted by figure 4.1. Stress and strain in a concrete slab's fibre are related to one another according to equations 4.2.1 [3]. The softening Young's modulus E_t which is assumed to correspond to the descending curve's secant [35] is represented in figure 4.2.

$$\sigma_t = E_c \varepsilon_t \quad \varepsilon_t \leq \varepsilon_{ct} \tag{4.2.1a}$$

$$\sigma_t = f_{ct}\left[1 - \frac{0.85(\varepsilon_t - \varepsilon_{ct})}{\varepsilon_1 - \varepsilon_{ct}}\right] \quad \varepsilon_{ct} < \varepsilon_t \leq \varepsilon_1 \tag{4.2.1b}$$

$$\sigma_t = 0.15 f_{ct}\frac{\varepsilon_u - \varepsilon_t}{\varepsilon_u - \varepsilon_1} \quad \varepsilon_1 < \varepsilon_t \leq \varepsilon_u \tag{4.2.1c}$$

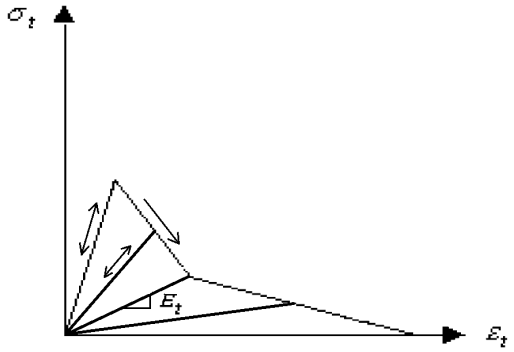

Figure 4.2: Softening elastic modulus.

4.3 Non-linear analysis

Since the constitutive law of concrete is non-linear, the internal forces in the concrete slab are no longer obtained directly from equation 2.3.11. Thus, the internal forces corresponding to an arbitrary displacement field must be evaluated through a numerical procedure. To this end, a non-linear algorithm consisting of a gradual imposition of load increments is adopted, until the total load acting on the structure is reached. For each load increment, the nodal displacements are obtained by resorting to the tangent stiffness matrix associated with the previous increment. Once the displacements and strain fields are known, the stress field can also be determined.

Due to the non-linear constitutive law, the nodal forces associated with the strain field do not correspond to the prescribed nodal loads and hence an unbalance arises. This unbalance is corrected through an iterative method, the so-called Newton-Raphson, by loading the structure with the unbalanced forces obtained in the previous iteration. Multiple iterations are carried out, within the same load increment, until a convergence criterion has been attained.

To better clarify the non-linear method implemented, a beam is considered to be subjected to concentrated loads $\mathbf{Q}$ and distributed loads $\mathbf{p}$. The loading is divided into load increments applied sequentially so that

when the last increment is applied the following loads act on the beam:

$$\mathbf{Q}^k = \mathbf{Q}^{k-1} + \Delta\mathbf{Q}^k \tag{4.3.1}$$

$$\mathbf{p}^k = \mathbf{p}^{k-1} + \Delta\mathbf{p}^k \tag{4.3.2}$$

In the same way, the final displacements of the structure are given by:

$$\mathbf{q}^k = \mathbf{q}^{k-1} + \Delta\mathbf{q}^k \tag{4.3.3}$$

in which

$$\Delta\mathbf{q}^k = \sum_{i=0}^{N} \Delta\mathbf{q}_i^k \tag{4.3.4}$$

The i index refers to iterative process within each load increment, N correspond to the number of iterations necessary to the method converge to the adopted criterion and $\Delta\mathbf{q}_i^k$ represents the nodal displacements variation within iteration i within increment k. The whole iterative process is summarised graphically in figure 4.3.

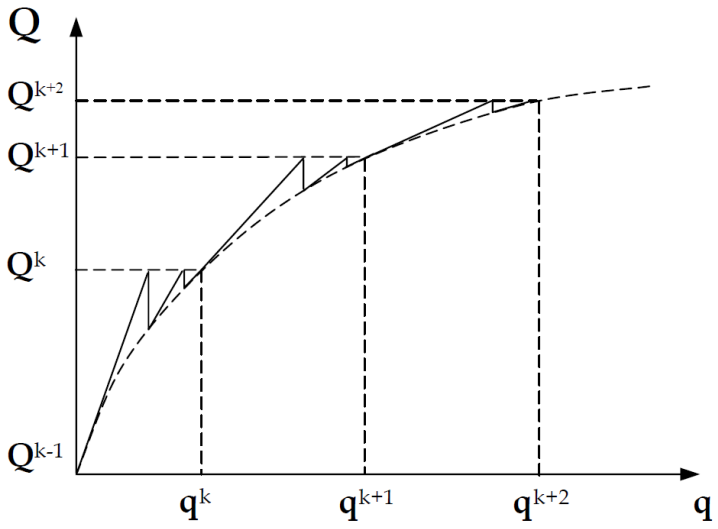

Figure 4.3: Incremental and iterative process at the structure level (adapted from [4]).

It is worth noting that, for the sake of simplicity, the explanation of this method is focused on a single beam element. Whenever the structure is discretised in multiple finite elements, assembling operations must be performed according to all structure's degrees of freedom.

At a given iteration, i, of the load increment k, the variation of the nodal displacements is evaluated through the following expression:

$$\mathbf{K}_{e,i}^{k} \Delta \mathbf{q}_{i}^{k} = \Delta \tilde{\mathbf{Q}}_{i}^{k} \tag{4.3.5}$$

being $\mathbf{K}_{e,i}^{k}$ the tangent stiffness matrix corresponding to the iteration i within the load increment k, which is defined by equation 3.2.16, i.e., $\mathbf{K}_{e,i}^{k}$ is determined as function of the deformation associated with displacements $\mathbf{q}_{i}^{k}$. The vector $\Delta \tilde{\mathbf{Q}}_{i}^{k}$ represents the nodal forces, corresponding to iteration i within the load increment k, accounting also for the statically equivalent nodal forces arising from distributed loads. $\Delta \tilde{\mathbf{Q}}_{i}^{k}$ is given by:

$$\Delta \tilde{\mathbf{Q}}_{i}^{k} = \Delta \mathbf{Q}_{i}^{k} + \Delta \mathbf{Q}_{0,i}^{k} \tag{4.3.6}$$

where $\Delta \mathbf{Q}_{i}^{k}$ represents the concentrated loads applied and $\Delta \mathbf{Q}_{0,i}^{k}$ represents the statically equivalent nodal forces which can be thought of as the symmetric of fixation forces.

By knowing the nodal displacements, $\mathbf{q}_{i}^{k}$, one can evaluate the strain field through compatibility conditions (equation 2.2.13) and, then, the stress field through the constitutive law (equation 2.2.21). Internal forces are obtained by integrating the stress field over the the beam's cross section. A nodal forces vector equilibrating these internal forces over the element's length is obtained by the following integral expression:

$$\mathbf{Q}_{ec} = \int_{0}^{L_e} \mathbf{B}^{T} \mathbf{s} \, dx \tag{4.3.7}$$

where the matrix $\mathbf{B}$ (equation 3.2.17) relates the vector of the deformation parameters to the vector of nodal displacements; and $\mathbf{s}$ represents the vector of internal forces.

It should be noticed that vector $\mathbf{Q}_{ec}$ corresponds to a single finite element. Assembling operations must be performed to obtained a global nodal forces vector, $\mathbf{Q}_{c}$, associated with the whole structure.

Because non-linear constitutive laws are adopted, the vector of equilibrated nodal forces on the structure, $\mathbf{Q}_{c}$, does not equal the external nodal loads vector defined in equation 4.3.6 for each iteration within an

increment, causing the following unbalanced loads:

$$\Delta \mathbf{Q}_{d,i}^{k} = \mathbf{Q}^{k} - \mathbf{Q}_{c,i}^{k} \tag{4.3.8}$$

The global tangent stiffness matrix is then updated, according to the beam's state of deformation. This process is graphically explained in figure 4.4, where the slope, corresponding to the stiffness matrix, is set to be tangent at each point starting a new iteration i. On the following iterations $(i+1, i+2, ..., N)$ within the load increment k, equation 4.3.5 is replaced by:

$$\mathbf{K}_{g,i}^{k} \Delta \mathbf{q}_{i}^{k} = \Delta \mathbf{Q}_{d,i}^{k} \tag{4.3.9}$$

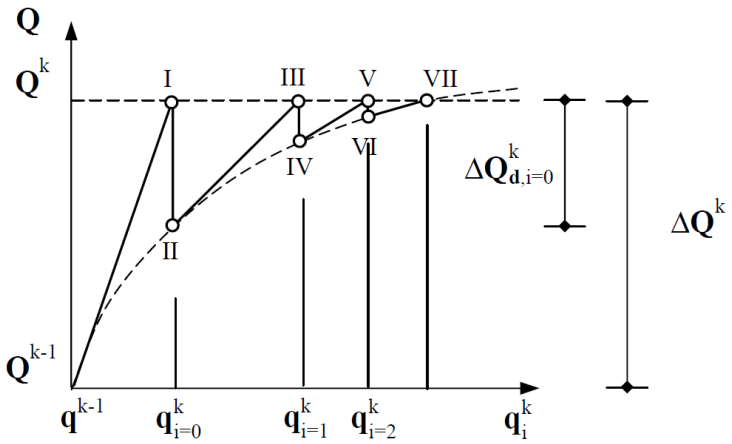

Figure 4.4: Incremental and iterative process of the whole structure within load increment k (adapted from [4]).

The unbalance, obtained by equation 4.3.8, tends to be null as the procedure is repeated. In figure 4.4, the line segments $(I-II, III-IV, V-VI)$ representing the unbalanced forces are successively smaller. The iterative process within the load increment k is assumed to have converged when the unbalance, calculated in equation 4.3.8, becomes approximately null, that is to say, whenever the following criterion is satisfied.

$$|\Delta \mathbf{Q}_{d,i}^{k}| < err = 1‰ \tag{4.3.10}$$

where err stands for admissible relative error and is given by:

$$err = \frac{\Delta \mathbf{Q}_{d,i}^{k}}{\Delta \mathbf{Q}^{k}} = \frac{\mathbf{Q}^{k} - \mathbf{Q}_{c,i}^{k}}{\Delta \mathbf{Q}^{k}} \tag{4.3.11}$$

The cycle goes through the next load increment, $k+1$, and the whole process is repeated as many times as the prescribed number of load increments.

The flow chart describing the algorithm of implementation of the Newton-Raphson method is represented in figure 4.5.

4.4 Comparison with experimental data

The non-linear model was adopted to evaluate the influence of concrete's cracking and shear connection deformation on the structural behaviour of composite beams. To be used as a reliable tool of analysis the model's accuracy is verified by comparing its results with experimental data. In this section, four different beams are considered, two simply-supported beams and two continuous beams with two spans.

It is worth mentioning that the numerical model developed in this work remains valid only for the structural steel linear range, since no plasticity was considered for steel's constitutive law.

4.4.1 Simply supported beams

Two simply supported beams corresponding to those tested by Chapman and Balakrishnan [6] were analysed using the proposed numerical model. Both beams have a 5.490 m long span, a hot rolled I-shaped steel beam 12"×6"×44 lb/ft BSB (British Standard Beam) and a concrete slab 0.152 m thick and 1.220 m wide, as represented in figure 4.6). Beam E1 is subjected to a midspan concentrated load, whereas beam U4 is subjected to a uniformly distributed loading. Shear connectors were disposed according to shear flow elastic longitudinal distribution. Thus, two rows of headed studs with 12.7 mm of diameter and 50 mm height are equally distributed at 120 mm along beam E1's length, whereas beam U4 has headed studs with 19 mm of diameter and 102 mm height linearly distributed over its interface connection.

Because both beams allow symmetry simplifications, meshes with four elements per half span were adopted in numerical tests. Shear connectors were assumed to be uniformly distributed along each finite element's length.

A comparison between experimental and numerical results for load versus midspan deflection curves for beams E1 and U4 is represented in figures 4.7 and 4.8. It can be observed the good agreement between experimental and numerical results. The small discrepancies can be due to the contact bond acting at the steel-concrete interface which was neglected [5, 6].

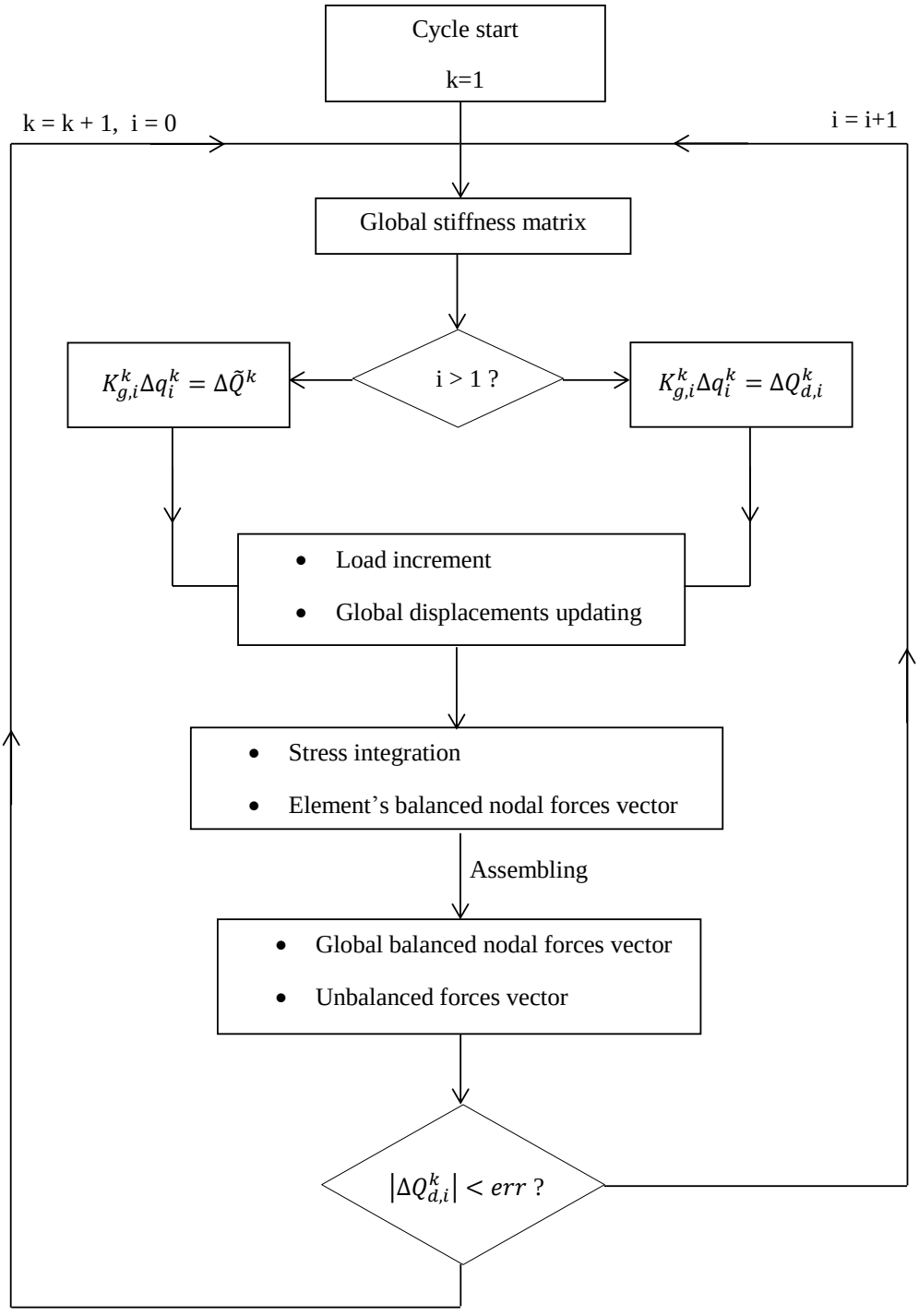

Figure 4.5: Flow chart of the non-linear analysis method.

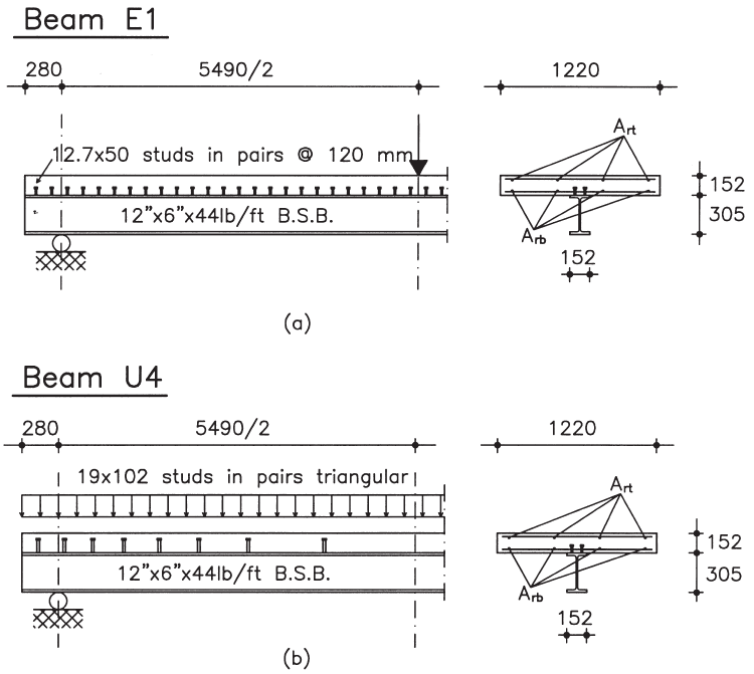

Figure 4.6: Geometrical properties of simply supported beams (adapted from [5, 6]).

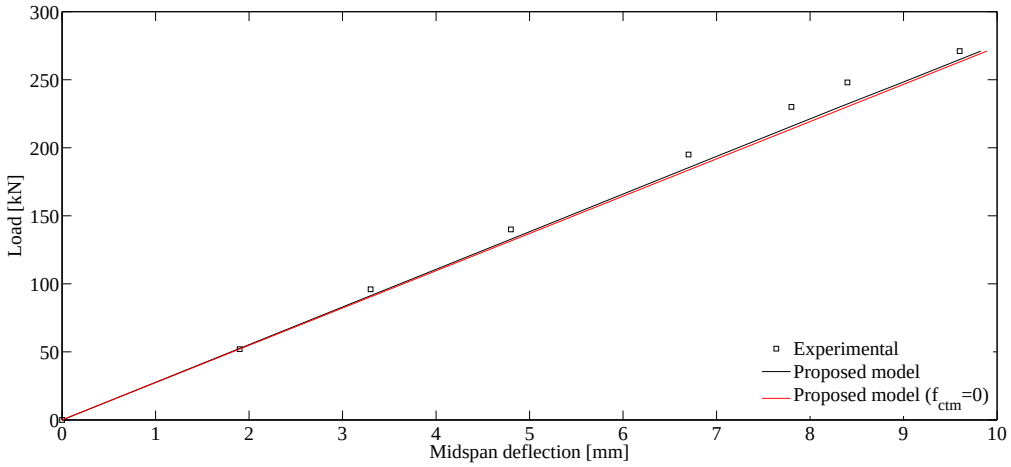

Figure 4.7: Comparison between experimental and numerical results of load-deflection curve for beam E1.

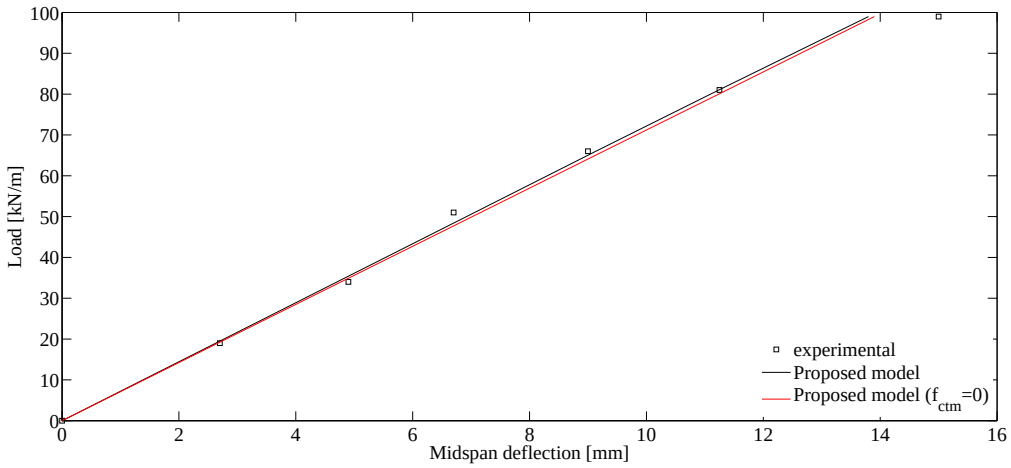

Figure 4.8: Comparison between experimental and numerical results of load-deflection curve for beam U4.

4.4.2 Two-span continuous beams

Beams CTB3 and CTB4, tested by Ansourian [11], were considered in order to verify the numerical model's accuracy on the hogging region. Both beams are represented in figure 4.9.

Either beam CTB3 or beam CTB4 have two equal spans of 4.5 m, a hot rolled H-shaped steel beam HEA 200 and three rows of headed stud connectors with 19 mm of diameter and 75 mm height equally spaced at 350 mm over the beam except over the hogging region, 1.050 m for both sides of the internal support, where the spacing between connectors decrease to 300 mm. Beam CTB3's concrete slab has a thickness of 0.100 m and a breadth of 1.300 m, whereas beam CTB4 possesses one with 0.100 m of thickness and 0.800 m of breadth. Either beam CTB3 or beam CTB4 are loaded with symmetrical midspan concentrated loads.

Again, symmetry simplifications are applied in order to gain computational efficiency, and meshes of four elements per span are employed.

The experimental and numerical results of deflection and curvature at midspan and curvature at the internal support varying with the load acting on beam CTB3 are represented in figures 4.10 and 4.11. It should be mentioned that the hogging curvature was not measured right at the support section but at 150 mm from it [5, 14]. It can be noticed that both curves, experimental and numerical, are very close, mainly in what regards load versus deflection and load versus support curvature, which certify the reliability of the proposed model.

A comparison between experimental and numerical results for beam CTB4, namely the curves of load versus midspan deflection and load versus support curvature, is presented in figures 4.12 and 4.13, respectively. The hogging curvature was also measured at 150 mm from the internal support. Again, experimental and

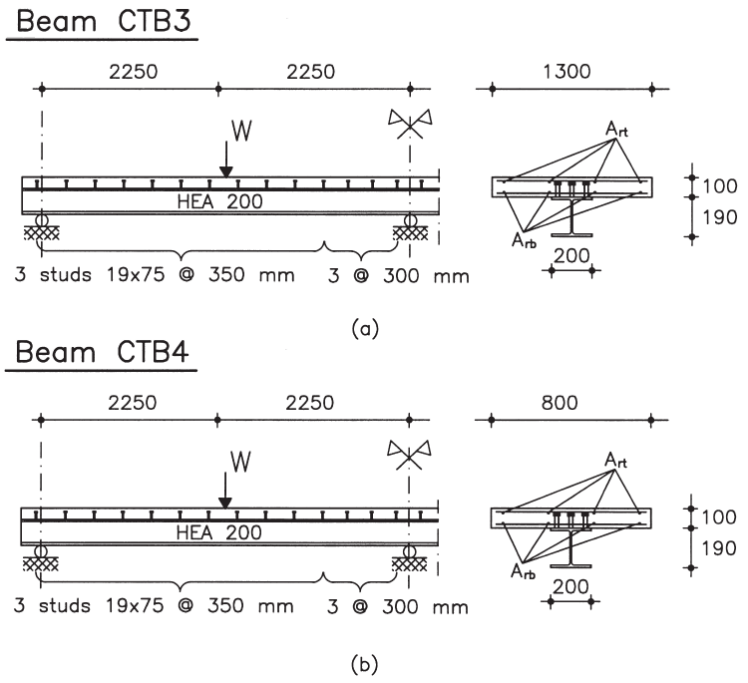

Figure 4.9: Geometrical properties of continuous beams (adapted from [5, 6]).

numerical curves are in a good agreement, confirming the ability of the proposed model to study the influence of structural concrete's cracking and of connection deformation in composite beams global response.

4.5 Applications

In this section an illustrative example of a continuous composite beam is solved in order to compare the numerical results from the proposed model with the results obtained by following the guidelines given by EN 1994-1-1.

A composite floor is admitted to be constituted by a concrete slab supported by steel beams placed with a spacing of 3.5 m and with two 10 m long spans. The composite action is assumed to be complete in order to isolate the influence of the concrete flange's cracking.

The composite cross section is formed by a rectangular concrete slab of class C25/30 with a thickness of 150 mm and with a effective width, due to shear lag, of 2225 mm in regions of sagging bending (resulting from the application of the clause 5.4.1.2 from EN1994-1-1); and by a doubly-symmetric plate girder of grade S355 with 440 mm of depth, 20 mm of flange's thickness and 10 mm of web's thickness. The geometrical properties of the cross section of the beam is presented in figure 4.14.

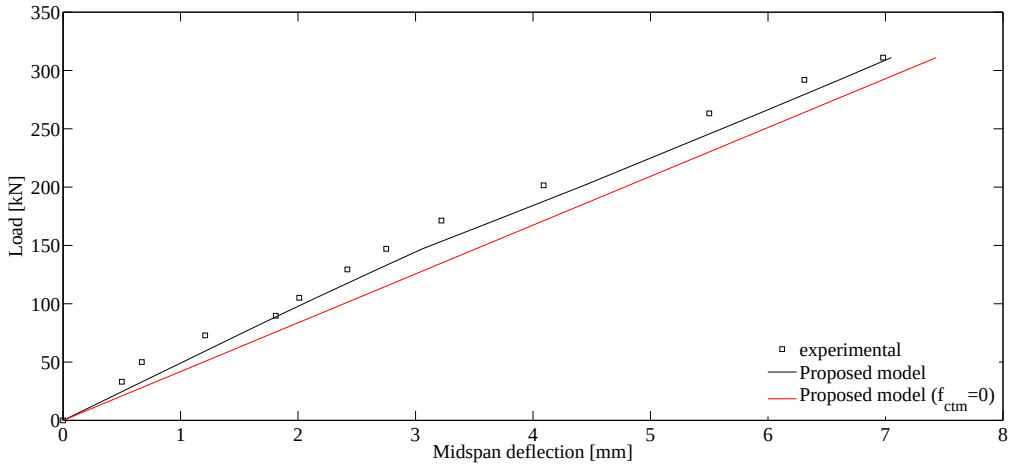

Figure 4.10: Comparison between experimental and numerical results of load-deflection curve for beam CTB3.

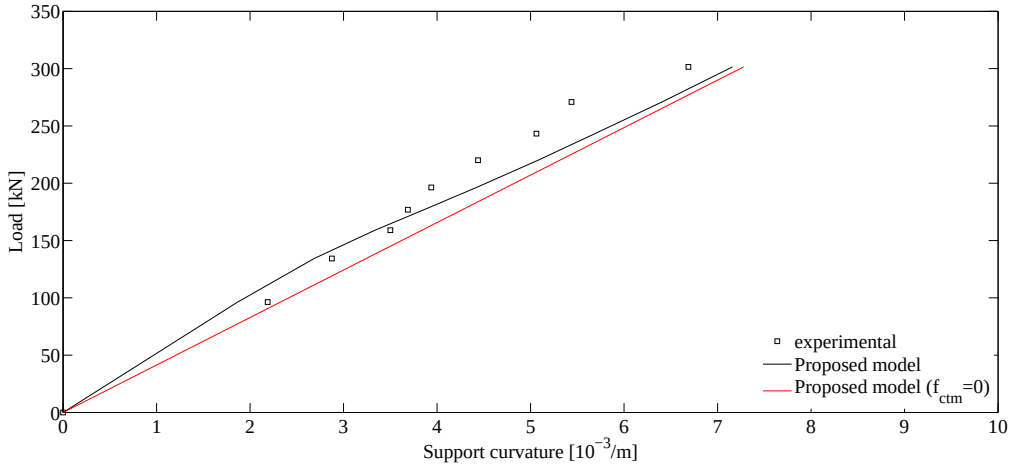

Figure 4.11: Comparison between experimental and numerical results of load versus support curvature curve for beam CTB3.

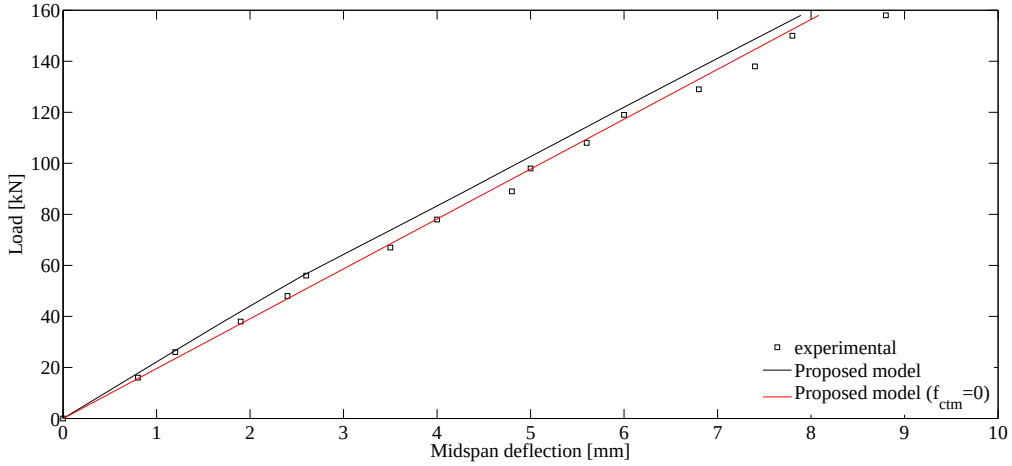

Figure 4.12: Comparison between experimental and numerical results of load-deflection curve for beam CTB4.

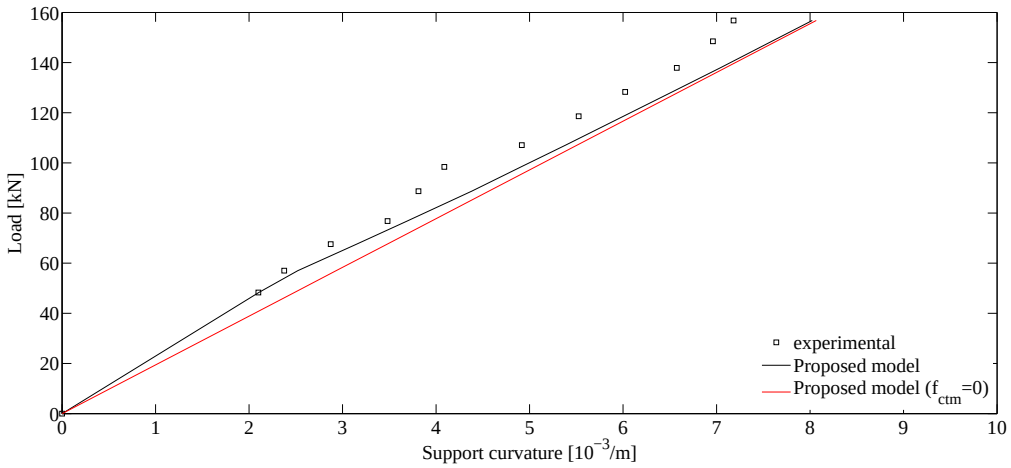

Figure 4.13: Comparison between experimental and numerical results of load versus support curvature curve for beam CTB4.

A symmetry simplification was considered in order to save computational time and gain efficiency. Thus, the two-span continuous beam is reduced to a single span beam and its inner support is substituted by a built-in end.

The effect of cracking in a continuous beam with concrete slab can be taken into account by adopting a cracked flexural stiffness $E_a I_2$ over 15% of the span on each side of the internal support and an un-cracked stiffness $E_a I_1$ on the 85% remaining, according to clause 5.4.2.3(3) from EN 1994-1-1. To apply this method the relation between adjacent spans should be higher than 0.6.

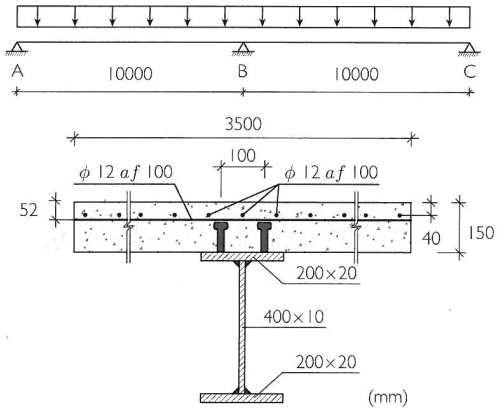

Figure 4.14: Composite cross section (adapted from [7]).

The values presented in table 4.1 were obtained for the bending moment over the internal support, midspan deflection and x-coordinate from which the concrete slab is totally cracked, by applying both the proposed non-linear model and the un-cracked linear elastic analysis, in which the length of the cracked region was defined, *a priori*, according to Eurocode's procedure.

Table 4.1: Comparison between the clause 5.4.2.3(3) from EN 1994-1-1 and the proposed model.

	Eurocode's method	Proposed model ($f_{ctm} = 0$)	Proposed model
Moment at support [kNm]	293.8	275.2	347.4
Midspan deflection [mm]	7.3	8.4	6.1
x-coordinate [m]	8.5	8.25	-

The comparison between values provided by different methods, in this case, leads to the conclusion that, in the domain of SLS, Eurocode's method tends to be a little conservative in what regards the influence of the concrete flange's cracking, since it results in a greater mid-span deflection. The influence of the tension stiffening on the hogging region appears to be non-negligible, once the moment redistribution and the mid-span deflection are significantly smaller, comparing with the two other methods not considering that effect.

Chapter 5

Concluding remarks and future developments

The present dissertation investigates the influence of the shear connection deformation and of the cracking of the concrete flange over the hogging region in the global response of composite beams.

An analytical model, based on Newmark's hypotheses, was formulated, by establishing equilibrium equations, compatibility conditions and constitutive laws. The system of differential equations governing the problem of partial interaction in composite beams was solved and a parametric study regarding the shear connection stiffness was performed.

Thereafter, a finite element approximating the displacement field was formulated in order to provide a reliable tool of analysis of the stress redistribution between the concrete flange and the steel beam caused by the shear connection deformation and by the concrete's cracking.

The results obtained with the linear numerical model were compared with the analytical solution for different values of the shear connection stiffness. The effectiveness of the proposed finite element model was ensured by the good agreement between numerical results and analytical solutions. Moreover, the numerical model has presented a good convergence rate to the analytical solution as the mesh refinement increased.

The influence of the connection stiffness in composite beams' behaviour is manifested by vertical displacements and by redistributions of either axial stress on the composite cross-section or shear flow along the connection interface.

Finally, a non-linear constitutive law for concrete under tension was adopted and the algorithm underly-

ing its implementation, the so-called Newton-Raphson method, was explained.

It was concluded that a higher shear connection stiffness, i.e., a larger composite action between steel and concrete, results in lower displacements. Thus, constraining the longitudinal slip between steel and concrete significantly contributes to reduce vertical displacements of composite beams. In the hogging region, the cracking of the concrete flange causes a redistribution of stress from concrete to steel, increasing the flexibility of the composite beam. The tension stiffening effect has proved to be not negligible for a limited load range.

Experimental tests available in literature were used as benchmark in order to validate the non-linear finite element model proposed. The good agreement between numerical and experimental results proved the ability of this method to study composite beams with partial interaction even when accounting for concrete's non-linear behaviour over the hogging region.

At last, some suggestions aiming at future developments of the present work are proposed:

- Study of the ULS on composite beams, by taking into account the steel's plasticity and shear connectors' non-linear constitutive relation;
- Analysis of composite beams with longitudinal and transverse partial interaction, i.e., to evaluate the influence of uplift on the overall behaviour;
- Analysis of the influence of time-dependent effects on the global response of composite beams with deformable connection;
- Geometrical non-linear analysis of composite beam-columns;
- Analysis of pre-stressed composite beams;

Bibliography

[1] G. Ranzi, F. Gara, and P. Ansourian, "General method of analysis for composite beams with longitudinal and transverse partial interaction," *Computers & structures*, vol. 84, no. 31, pp. 2373–2384, 2006.

[2] J. Fish and T. Belytschko, *A first course in finite elements*. John Wiley and Sons, 2007.

[3] X. Wang and X. Liu, "A strain-softening model for steel–concrete bond," *Cement and concrete research*, vol. 33, no. 10, pp. 1669–1673, 2003.

[4] R. Vieira, "Análise de vigas mistas: influência da deformabilidade da conexão e dos efeitos diferidos," Master's thesis, Instituto Superior Técnico, Universidade Técnica de Lisboa, 2000 [in Portuguese].

[5] N. Gattesco, "Analytical modeling of nonlinear behavior of composite beams with deformable connection," *Journal of Constructional Steel Research*, vol. 52, no. 2, pp. 195–218, 1999.

[6] J. Chapman and S. Balakrishnan, "Experiments on composite beams," *The Structural Engineer*, vol. 42, no. 11, pp. 369–383, 1964.

[7] L. Calado and J. Santos, "Estruturas mistas de aço e betão," 2009.

[8] J. Aribert and K. Abdel Aziz, "Calcul des poutres mixtes jusqu'à l'état ultime avec un effet de soulèvement à l'interface acier-béton," *CONSTR MET*, no. 4, 1985.

[9] R. Johnson and I. May, "Partial-interaction design of composite beams," *Structural Engineer*, vol. 8, no. 53, 1975.

[10] N. M. Newmark, C. P. Siess, and I. Viest, "Tests and analysis of composite beams with incomplete interaction," *Proc Soc Exp Stress Anal*, vol. 9, no. 1, pp. 75–92, 1951.

[11] P. Ansourian, "Experiments on continuous composite beams.," in *ICE Proceedings*, vol. 73, pp. 26–51, Thomas Telford, 1982.

[12] A. Adekola, "Partial interaction between elastically connected elements of a composite beam," *International Journal of Solids and Structures*, vol. 4, no. 11, pp. 1125–1135, 1968.

[13] U. A. Girhammar and V. K. Gopu, "Composite beam-columns with interlayer slip-exact analysis," *Journal of Structural Engineering*, vol. 119, no. 4, pp. 1265–1282, 1993.

[14] H. Loh, B. Uy, and M. Bradford, "The effects of partial shear connection in the hogging moment regions of composite beams part ii—analytical study," *Journal of Constructional Steel Research*, vol. 60, no. 6, pp. 921–962, 2004.

[15] Q.-H. Nguyen, E. Martinelli, and M. Hjiaj, "Derivation of the exact stiffness matrix for a two-layer timoshenko beam element with partial interaction," *Engineering Structures*, vol. 33, no. 2, pp. 298–307, 2011.

[16] M. R. Salari, E. Spacone, P. B. Shing, and D. M. Frangopol, "Nonlinear analysis of composite beams with deformable shear connectors," *Journal of Structural Engineering*, vol. 124, no. 10, pp. 1148–1158, 1998.

[17] A. Ayoub and F. C. Filippou, "Mixed formulation of nonlinear steel-concrete composite beam element," *Journal of Structural Engineering*, vol. 126, no. 3, pp. 371–381, 2000.

[18] A. Dall'Asta and A. Zona, "Three-field mixed formulation for the non-linear analysis of composite beams with deformable shear connection," *Finite Elements in Analysis and Design*, vol. 40, no. 4, pp. 425–448, 2004.

[19] L. Dezi and A. M. Tarantino, "Creep in composite continuous beams. i: Theoretical treatment," *Journal of Structural Engineering*, vol. 119, no. 7, pp. 2095–2111, 1993.

[20] C. Faella, E. Martinelli, and E. Nigro, "Steel–concrete composite beams in partial interaction: Closed-form "exact" expression of the stiffness matrix and the vector of equivalent nodal forces," *Engineering Structures*, vol. 32, no. 9, pp. 2744–2754, 2010.

[21] C. Amadio and M. Fragiacomo, "A finite element model for the study of creep and shrinkage effects in composite beams with deformable shear connections," *Costruzioni Metalliche*, vol. 4, pp. 213–228, 1993.

[22] G. Ranzi and M. Bradford, "Analytical solutions for the time-dependent behaviour of composite beams with partial interaction," *International journal of solids and structures*, vol. 43, no. 13, pp. 3770–3793, 2006.

[23] R. Vieira and F. Virtuoso, "Analysis of steel-concrete beams: Influence of time dependent effects, cracking and connection flexibility," 2012.

[24] G. Ranzi, A. Dall'Asta, L. Ragni, and A. Zona, "A geometric nonlinear model for composite beams with partial interaction," *Engineering Structures*, vol. 32, no. 5, pp. 1384–1396, 2010.

[25] A. Zona and G. Ranzi, "Finite element models for nonlinear analysis of steel–concrete composite beams with partial interaction in combined bending and shear," *Finite Elements in Analysis and Design*, vol. 47, no. 2, pp. 98–118, 2011.

[26] A. Dall'Asta and A. Zona, "Non-linear analysis of composite beams by a displacement approach," *Computers & structures*, vol. 80, no. 27, pp. 2217–2228, 2002.

[27] F. Gara, G. Ranzi, and G. Leoni, "Displacement-based formulations for composite beams with longitudinal slip and vertical uplift," *International journal for numerical methods in engineering*, vol. 65, no. 8, pp. 1197–1220, 2006.

[28] J. Aribert, E. Ragneau, and H. Xu, "Développement d'un élément fini de poutre mixte acier-béton intégrant les phénomènes de glissement et de semi-continuité avec éventuellement voilement local," *Revue Construction Métallique*, vol. 2, pp. 31–49, 1993 [in French].

[29] J. Aribert, "Slip and uplift measurements along the steel and concrete interface of various types of composite beams," *E & FN Spon(UK),*, pp. 395–410, 1992.

[30] U. A. Girhammar and D. Pan, "Dynamic analysis of composite members with interlayer slip," *International journal of solids and structures*, vol. 30, no. 6, pp. 797–823, 1993.

[31] A. Razaqpur and M. Nofal, "A finite element for modelling the nonlinear behavior of shear connectors in composite structures," *Computers & Structures*, vol. 32, no. 1, pp. 169–174, 1989.

[32] J. N. Reddy, *An Introduction to the Finite Element Method*. McGraw-Hill Series in Mechanical Engineering, McGraw-Hill Education, 3rd ed., 2006.

[33] A. Dall'Asta and A. Zona, "Slip locking in finite elements for composite beams with deformable shear connection," *Finite Elements in Analysis and Design*, vol. 40, no. 13, pp. 1907–1930, 2004.

[34] R. Johnson, N. Molenstra, *et al.*, "Partial shear connection in composite beams for buildings.," in *ICE Proceedings*, vol. 91, pp. 679–704, Thomas Telford, 1991.

[35] J. Pina, *Structural assessment of corroded RC structures through numerical modelling*. PhD thesis, Instituto Superior Técnico, 2009.